THE JOURNAL OF BIOLOGICAL CHEMISTRY VOL. 292, NO. 6, pp. 2328–2344, February 10, 2017

Aggregation of Full-length Immunoglobulin Light Chains from Systemic Light Chain Amyloidosis (AL) Patients Is Remodeled by Epigallocatechin-3-gallate*[S]

Received for publication, July 25, 2016, and in revised form, December 22, 2016 Published, JBC Papers in Press, December 28, 2016, DOI 10.1074/jbc.M116.750323

Kathrin Andrich[‡§], Ute Hegenbart[¶], Christoph Kimmich[¶], Niraja Kedia[‡], H. Robert Bergen 3rd[‖], Stefan Schönland[¶], Erich Wanker[§], and Jan Bieschke[‡1]

From the [‡]Department of Biomedical Engineering, Washington University, St. Louis, Missouri 63130-4899, the [§]Max-Delbrück Center for Molecular Medicine in the Helmholtz Association, 13125 Berlin, Germany, the [¶]Department of Internal Medicine V (Hematology/Amyloidosis Center), University Hospital Heidelberg, 69120 Heidelberg, Germany, and the [‖]Translational PKD Center, Mayo Clinic, Rochester, Minnesota 55905

Edited by Paul E. Fraser

Intervention into amyloid deposition with anti-amyloid agents like the polyphenol epigallocatechin-3-gallate (EGCG) is emerging as an experimental secondary treatment strategy in systemic light chain amyloidosis (AL). In both AL and multiple myeloma (MM), soluble immunoglobulin light chains (LC) are produced by clonal plasma cells, but only in AL do they form amyloid deposits *in vivo*. We investigated the amyloid formation of patient-derived LC and their susceptibility to EGCG *in vitro* to probe commonalities and systematic differences in their assembly mechanisms. We isolated nine LC from the urine of AL and MM patients. We quantified their thermodynamic stabilities and monitored their aggregation under physiological conditions by thioflavin T fluorescence, light scattering, SDS stability, and atomic force microscopy. LC from all patients formed amyloid-like aggregates, albeit with individually different kinetics. LC existed as dimers, ~50% of which were linked by disulfide bridges. Our results suggest that cleavage into LC monomers is required for efficient amyloid formation. The kinetics of AL LC displayed a transition point in concentration dependence, which MM LC lacked. The lack of concentration dependence of MM LC aggregation kinetics suggests that conformational change of the light chain is rate-limiting for these proteins. Aggregation kinetics displayed two distinct phases, which corresponded to the formation of oligomers and amyloid fibrils, respectively. EGCG specifically inhibited the second aggregation phase and induced the formation of SDS-stable, non-amyloid LC aggregates. Our data suggest that EGCG intervention does not depend on the individual LC sequence and is similar to the mechanism observed for amyloid-β and α-synuclein.

Systemic light chain amyloidosis (AL)[2] is the most common form of systemic amyloidosis (1), but it is still a rare disease with an incidence of 6–7 in 1,000,000 people (2). Underlying AL pathology is a clonal plasma cell disorder, which produces an immunoglobulin light chain in the bone marrow with a unique sequence. These light chains are released into the blood (monoclonal gammopathy). When elevated LC levels in serum overwhelm renal absorption, LC is also found in the urine. Full-length LC can be isolated from the urine of these patients (3–5).

Clonal plasma cell disorders can present different types of pathologies; light chains form amyloid deposits in AL patients. Here, LC fibrils adopt a conformation characterized by highly stable, intramolecular cross-β-sheets that stain with Congo red (6) and thioflavin T (ThT) (7–9).

In contrast, amyloid deposits are not observed in patients suffering from multiple myeloma (MM), a malignant disease characterized by bone marrow failure and bone destruction. The two contrasting pathologies of LC gammopathies raise the question of which factors determine amyloid formation. Amyloid formation could be initiated (*a*) by the sequences of the individual light chains, (*b*) by high levels of light chain expression, (*c*) by posttranslational modification of the LC, (*d*) by fragmentation of the light chain, or (*e*) by a combination of these factors. A possible modification would be the formation or cleavage of intermolecular intradomain disulfide bonds.

The variable (V_L) and constant (C_L) domains of LC proteins are connected by a short joining domain (10–13). Both contain an intradomain disulfide bridge (10–15) between Cys-23 and Cys-104. Additionally, the constant domain can form interchain disulfide bonds to Ig heavy or light chains (10–13) via its conserved Cys-127 residue (16, 17).

Previous quantitative studies have focused on a small number of recombinant proteins spanning the variable domain of the LC proteins (18–26). These systems cannot address the relevance of interdomain interactions in LC amyloid formation.

* This work was supported by German Ministry for Science and Education (BMBF GERAMY) Grants 01GM1107C and 01GM1107A, by the Diabetes Research Center at Washington University (National Institutes of Health Grant No. 5, P30 DK020579), and by German Science Foundation (DFG) Grant BI 1409/1-1. The authors declare that they have no conflicts of interest with the contents of this article. The content is solely the responsibility of the authors and does not necessarily represent the official views of the National Institutes of Health.

[S] This article contains supplemental Figs. 1–4.

[1] To whom correspondence should be addressed. E-mail: bieschke@wustl.edu.

[2] The abbreviations used are: AL, systemic light chain amyloidosis; LC, light chain(s); ThT, thioflavin T; MM, multiple myeloma; EGCG, epigallocatechin-3-gallate; LDS, lithium dodecyl sulfate; GdnHCl, guanidine hydrochloride; aa, amino acids; HMW, high molecular weight; AFM, atomic force microscopy; HSA, human serum albumin; Aβ, amyloid-β.

TABLE 1
Summary of clinical data for AL and MM patients
IFE, immunofixation electrophoresis; NA, not applicable; GI, gastrointestinal.

Sample ID	Patient ID	Age (years)/ Gender	Type	IFE		Protein serum		Protein urine		Involved organs
				Serum	Urine	κ	λ	κ	λ	
						mg/liter		*mg/liter*		
κ-AL-1	35-12	59/femal	AL + MM	κ	κ	11,300	8	5,460	0	Soft tissue, GI tract
κ-AL-2	48-12	55/male	AL + MM	IgG κ	κ	3,750	1	4,242	6	Soft tissue
λ-AL-1	95-12	54/female	AL + MM	λ	λ	12	6,470	22	5,784	Soft tissue
λ-AL-2	66-12	66/male	AL + MM	λ	λ	6	654	0	265	Soft tissue, GI tract
κ-MM-1	344-13	64/male	MM	IgG κ	κ	2,173	5	3,400	0	NA
κ-MM-2	369-13	50/female	MM	κ	κ	33,209	1	2,437	3	NA
λ-MM-1	85-12	60/male	MM	IgA λ	λ	0	5,780	0	17,368	NA
λ-MM-2	448-13	47/female	MM	IgA λ	IgA, λ	0	1,495	0	9,016	NA
λ-MM-3	44-13	60/male	MM	λ	λ	18	2,050	36	2,100	NA

The significance of full-length LC for amyloid formation is not yet fully understood (27–30).

Our study, for the first time, quantifies stabilities and amyloid formation propensities of nine authentic, full-length LC proteins that we isolated from the urine of patients (4 with AL, 5 with MM). Our study tested whether AL and MM light chains had inherently different stabilities or amyloid formation propensities. We found that both AL and MM full-length light chains formed amyloid aggregates *in vitro*, but only under conditions that cleaved intermolecular disulfide bonds. Aggregation kinetics were unique for each LC protein and correlated only weakly with thermodynamic stability.

Treatment for the plasma cell clone pathology exists in the form of chemotherapy, but the direct treatment of amyloid pathology is still under investigation. Recently, we could show that the green tea polyphenol epigallocatechin-3-gallate (EGCG) redirects amyloid formation of amyloid-β and α-synuclein into inert amorphous aggregates (31–33). A case report of a patient who self-administered EGCG after several cycles of chemotherapy found that EGCG reduced LC deposits in the patient's heart and extended the patient's life over a period of several years (34). A reduction in cardiac pathology was observed in some but not all patients treated with EGCG (35). This observation raises the possibility that LC proteins from different patients may respond differently to EGCG.

Our study therefore tested the effect of EGCG on amyloid formation kinetics of our nine patient-derived LC proteins. We found that EGCG inhibited the conversion of oligomeric LC into ThT-positive fibrils and induced the formation of SDS-stable aggregates in all LC proteins.

Results

Purification of Ig Light Chains from Patient Urine—Utilizing a simple protocol, we purified nine monoclonal Ig light chains from the urine of patients. Patients displayed either MM pathology or AL pathology. AL patients also displayed MM markers in addition to AL pathology (AL + MM in Table 1). Instead of a standard dialysis approach (27, 36, 37), we utilized sequential membrane ultrafiltration, which removed small molecule components and concentrated the LC by a factor of 40–80 (Fig. 1*A*) (38). This protocol allowed us to parallelize the purification of a larger set of patient samples efficiently.

LC samples were analyzed via denaturing (DTT, heating to 95 °C, 2% lithium dodecyl sulfate (LDS)) and semidenaturing (no DTT, no heat, 2% LDS) SDS-PAGE (Fig. 1*B*). Each protein was analyzed by silver staining, showing the total protein amount (Fig. 1*B*, *lane t*), and by Western blotting against κ-isotype LC (Fig. 1*B*, *lane* κ), λ-isotype LC (Fig. 1*B*, *lane* λ), and human serum albumin (Fig. 1*B*, *lane a*), respectively.

Purified LC selected for further biochemical and biophysical analysis contained less than 6% albumin and came from patients with a minimum of 265 mg of LC/24 h of secretion in urine (Table 1). These samples showed at most a weak 67 kDa band in silver staining (Fig. 1*B*, *lane t*) that was confirmed as albumin by immunostaining (Fig. 1*B*, *lane a*).

The isolated LC proteins each were of a single isotype that ran in SDS-PAGE as single bands with apparent molecular masses of 24–28 kDa. Under non-reducing conditions, both monomers and S-S-linked dimers were present. Densitometric analysis of silver-stained proteins found 46 ± 11% of LC dimers. However, analysis by blue native PAGE (Figs. 4*B* and 5*A*), size exclusion chromatography, and dynamic light scattering (data not shown) revealed that the light chain proteins did not, in fact, present as free monomer and dimers, as suggested by SDS-PAGE analysis. Rather, LC ran as distinct di- and oligomeric species between 50 and 600 kDa, suggesting the formation of non-SDS-stable multimers built from LC monomers and dimers. Purification of LC by an alternative dialysis protocol yielded di- and oligomers identical to those yielded by our membrane filtration protocol (Fig. 1*C*). These data confirm that oligomeric LC species were present in the patient urine and not a result of our purification protocol. Strikingly, light chains largely ran as monomers in native PAGE after reduction with DTT (100 mM; Fig. 1*D*), suggesting that reduction of intermolecular disulfide bonds destabilized LC oligomers.

Secondary Structure and Thermal Stability of Light Chains—When analyzed by CD spectroscopy, LC proteins exhibited the expected β-sheet structure (Fig. 2, *A* and *B*) (39, 40). CD spectra could be grouped into κ- (Fig. 2*A*) and λ-isotype (Fig. 2*B*) LC (41). However, we observed no systematic differences between samples coming from MM or AL patients.

We then tested whether the stability of LC correlated with MM or AL pathology by recording thermal denaturation curves of the nine LC proteins (Fig. 2, *C* and *D*). Results are summarized in Table 2. Similar to the CD spectra, the melting points (T_m) grouped according to the LC isotypes (Table 1; κ-LC T_m = 48.6–51.6 °C, λ-LC T_m = 55.3–61.5 °C) with the exception of

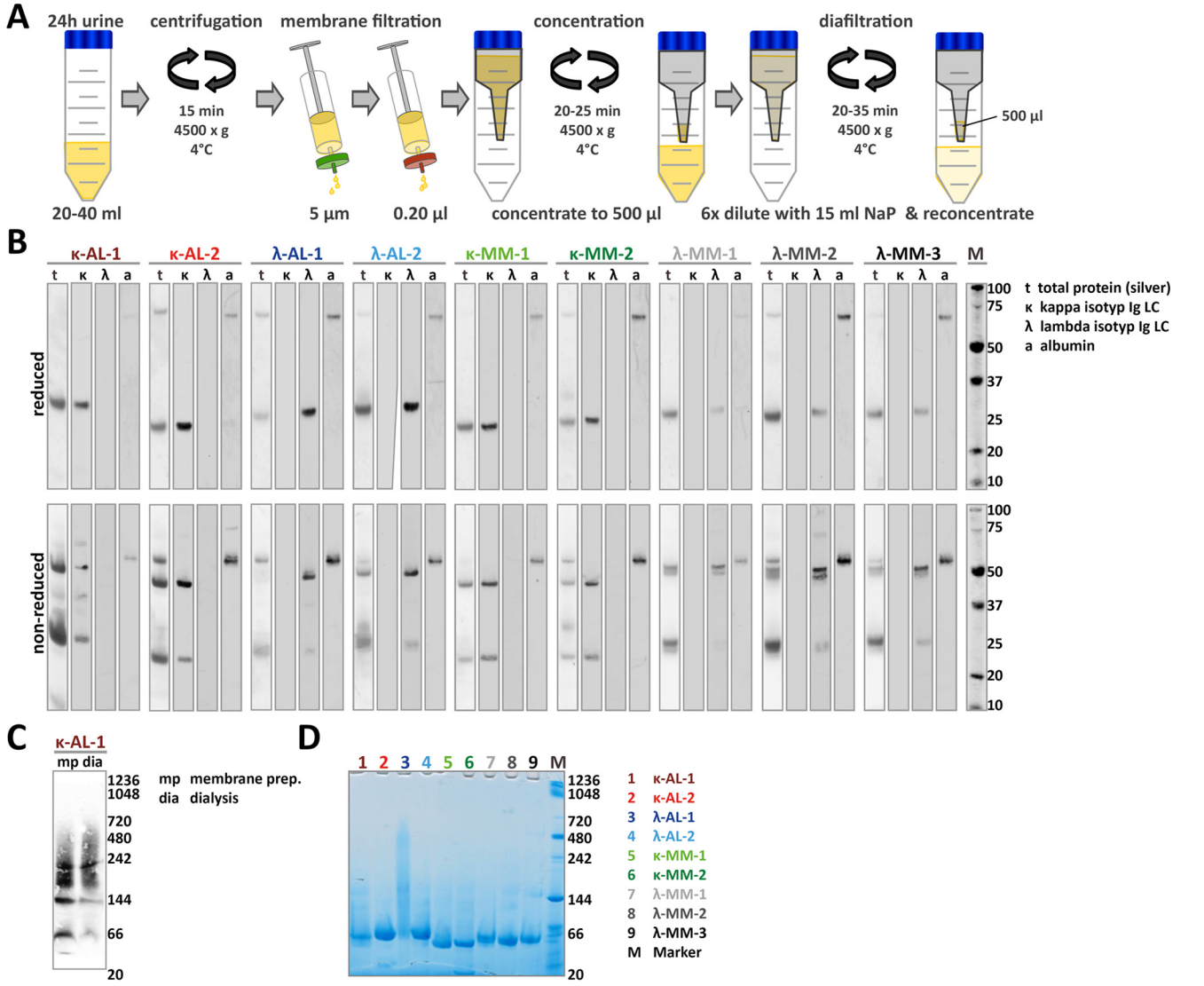

FIGURE 1. *A*, purification of Ig light chains from urine of patients diagnosed with AL or MM. *B*, denaturing and semidenaturing SDS-PAGE with silver staining for total protein (*t*) and Western blotting analysis for κ-LC (κ), λ-LC (λ), and human serum albumin (*a*). *C*, native PAGE Western blotting of κ-AL light chain urine sample purified by two alternative protocols, membrane filtration or dialysis. Both purification protocols yielded identical patterns of di- and oligomeric LC. *D*, Coomassie-stained native PAGE of light chain samples. LC (100 μM) were treated with DTT (100 mM) for 30 min in NaP buffer, diluted to 40 μM, and analyzed by blue native PAGE. Reduction removed HMW oligomers.

the κ-MM-1 (T_m = 60.4 °C, *light green*), which had a higher thermal stability than other κ-LC. These data suggest that the κ- and λ-isotypes of constant domains have a stronger influence on the overall LC stability than the individual variable domains (42). Reduction of LC with DTT under native conditions had little effect on stability (Fig. 2*E*). In contrast, reduction under denaturing conditions reduced thermal stability by ~12 °C (Fig. 2*E*). These results are consistent with literature data comparing the effect of inter- *versus* intramolecular disulfide bonds on LC stability (43). The results also indicate that only intermolecular disulfide bonds were reduced under the conditions of our aggregation assay.

We observed a temperature gradient-dependent hysteresis of 2.6–7.7 °C between denaturation and renaturation curves (data not shown). This behavior has been described for recombinant V_L domains and full-length LC (44). Although no obvious differences in thermal stability between AL and MM LC were observed during denaturation, λ-MM proteins did not renature into their native fold. These LC irreversibly formed aggregates after prolonged denaturation (not shown). Denaturation of all other LC proteins was at least partially (45–80%) reversible. This difference may reflect a difference in unfolding and aggregation pathways between light chains in AL and MM patients.

Thermodynamic Stabilities of Light Chains—We determined the free energies of unfolding via guanidine hydrochloride (GdnHCl) denaturation and monitored unfolding via tryptophan fluorescence (14, 15, 45–48) (Fig. 3*A*). The V_L and C_L domains contain a conserved tryptophan in position 41, the λ-isotype C_L domain contains an additional conserved Trp-96, and 0–4 non-conserved Trp residues may be present (16, 17). Fluorescence spectra exhibited both changes in intensity and shifts of the emission maximum on unfolding (Fig. 3, *A* and *B*). We incubated all samples at 6 M GdnHCl overnight and then

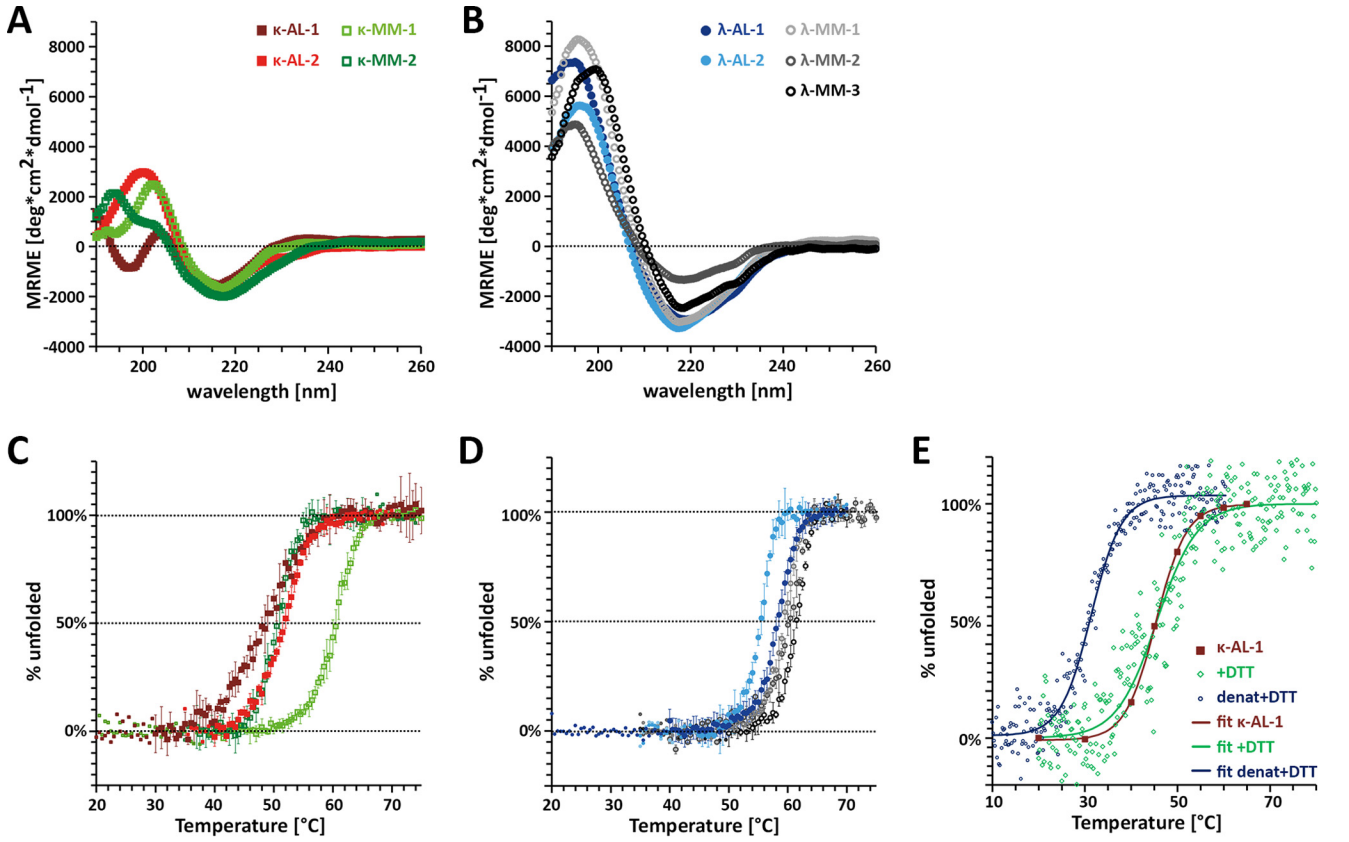

FIGURE 2. *A* and *B*, CD spectra of purified κ-isotype and λ-isotype LC. *C* and *D*, thermal denaturation curves (heating rate 0.5 °C/min); apparent melting points (T_m) for κ-LC of 48.6–51.6 °C (κ-MM-1, T_m = 60.4 °C) and for λ-LC of 55.3–61.5 °C; see Table 2 for detailed data. *E*, thermal denaturation of κ-AL-1 LC measured without denaturation (native, T_m = 46 ± 0.5 °C), after reduction of the intermolecular disulfide bonds under native conditions (+*DTT*, T_m = 43 ± 1 °C), or after reduction of inter- and intramolecular disulfide bonds in the GdnHCl denatured state (*denat* + *DTT*, T_m = 31 ± 0.5 °C).

TABLE 2

Summary of thermodynamic parameters and apparent molecular weights of Ig light chain proteins

NA, not applicable; ND, not determined; Max., maximum.

		GdnHCl denaturation						Thermal denaturation		SDS-PAGE
						Max. Trp fluorescence				
Sample	% final HSA[a]	Refolding[b]	c_m unfolding[c]	ΔG_0 unfolding	ΔG_0 refolding	Before	After	Refolding[b]	$T_{m(app)}$[d]	Apparent mass[e]
	%	%	M	kJ	kJ	nm		%	°C	kDa
κ-AL-1	0.3	100	1.0 ± 0.05	9 ± 1	ND		350	71	48.6 ± 0.2	24
κ-AL-2	3.6	100	2.2 ± 0.05	10 ± 1	ND	344	349	>50	51.6 ± 0.1	26
λ-AL-1	5.8	100	1.2 ± 0.05	10 ± 1	11 ± 5	338	350	87	58.3 ± 0.1	26
λ-Al-2	2.2	92	1.9 ± 0.05	14 ± 3	ND	331	349	59	55.3 ± 0.1	28
κ-MM-1	0.8	100	1.5 ± 0.05	14 ± 1	ND		350	75	60.4 ± 0.1	25
κ-MM-2	2.1	100	1.3 ± 0.05	13 ± 1	ND	346	349	66	50.5 ± 0.1	26
λ-MM-1	0.4	84	1.3 ± 0.05	17 ± 2	NA	320[f]	349	3	59.3 ± 0.1	27
λ-MM-2	3.5	78	1.6 ± 0.05	14 ± 1	NA	326[f]	348	7	60.2 ± 0.1	27
λ-MM-3	4.3	83	1.6 ± 0.05	16 ± 5	NA	325[f]	350	7	61.5 ± 0.1	28

[a] Final HSA determined in purified sample.
[b] Determined from CD data.
[c] Denaturant concentration at 50% unfolding.
[d] Apparent melting temperature determined with a heating rate of 0.5 K/min.
[e] Apparent molecular mass determined from reducing SDS-PAGE.
[f] For these samples, no distinct pre-transition peak position was found, and the Trp fluorescence intensity ratio at the indicated wavelengths was analyzed instead.

diluted the sample to 0.025 M GdnHCl to test for reversibility of unfolding (supplemental Fig. 1). CD spectra indicated that LC refolded into a native-like conformation (Table 2 and supplemental Fig. 1).

We analyzed denaturation and renaturation data for the λ-AL-1 light chain recorded by Trp fluorescence and by CD spectroscopy in more detail (Fig. 3, *C* and *D*). Unfolding energies (10 ± 1 kJ/mol) and refolding energies (−11 ± 5 kJ/mol) measured by fluorescence and by CD (13 ± 5 kJ/mol) were identical within experimental error. This indicated that unfolding was fully reversible and could be measured by both methods with similar accuracy.

We then analyzed unfolding data of our nine light chains (Fig. 3, *E* and *F*); all denaturation data are summarized in Table 2. κ-MM light chains were slightly more stable (13 ± 1 kJ/mol, and 14 ± 1 kJ/mol) than the κ-AL samples (9 ± 1 and 10 ± 1 kJ/mol). Similarly, λ-MM light chains (λ-MM-1, 17 ± 2 kJ/mol; λ-MM-2, 14 ± 1 kJ/mol; and λ-MM-3, 16 ± 5 kJ/mol) were

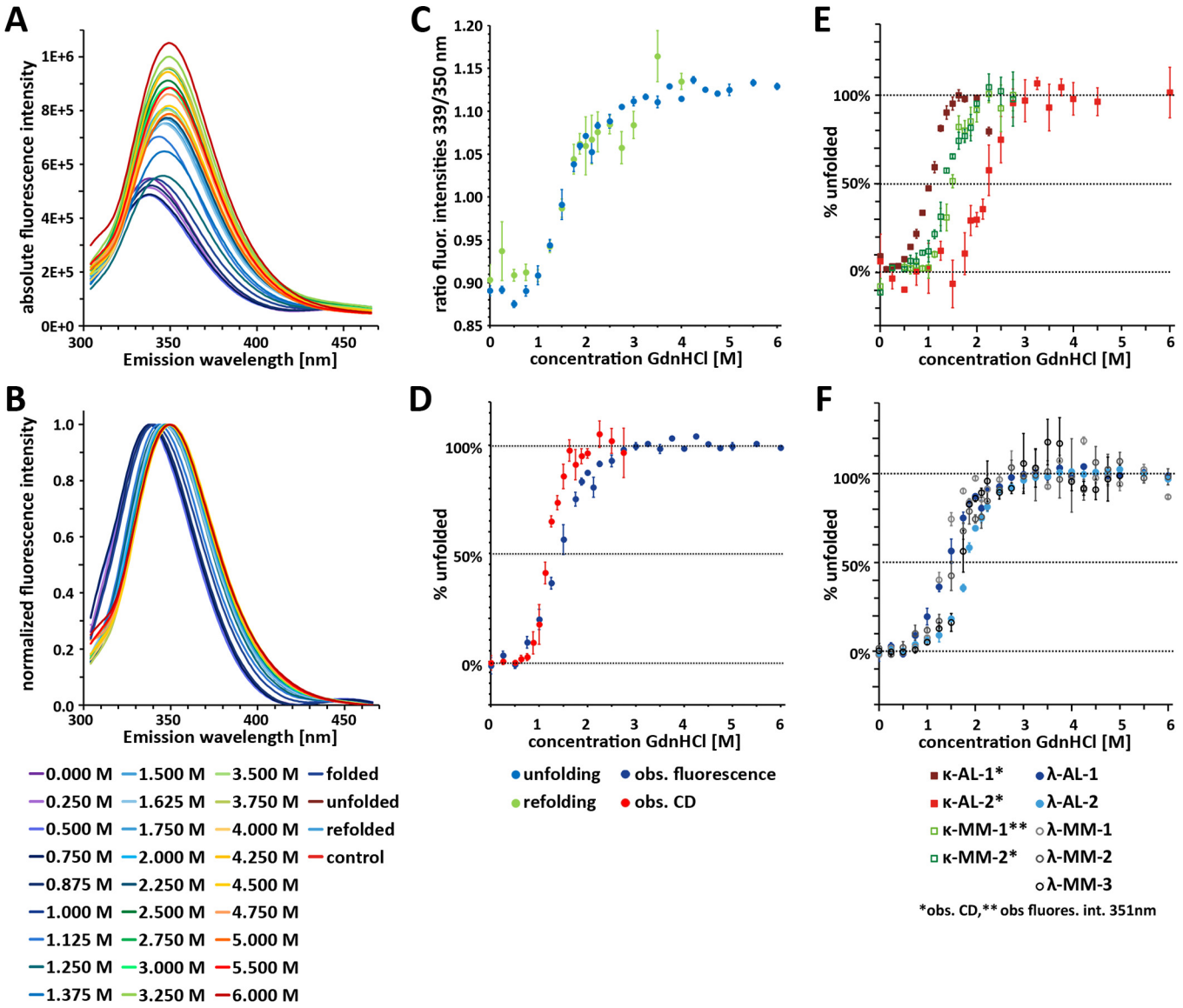

FIGURE 3. **GdnHCl denaturation data.** *A*, absolute intensity Trp fluorescence spectra of λ-AL-1 light chain. *B*, Trp fluorescence spectra of λ-AL-1 normalized to fluorescence maximum. *C*, unfolding (*blue*) and refolding (*light green*) curves as a function of GdnHCl concentration analyzed from the ratio of Trp fluorescence intensities at 339 and 350 nm, respectively. *D*, comparison of unfolding curves from fluorometric (*dark blue*) and CD spectroscopic data (*red*). *E* and *F*, unfolding curves of all κ-LC (*E*) and all λ-LC (*F*). Curves for λ-LC and κ-AL-2 are derived from Trp fluorescence data; other κ-LC curves are derived from CD signals at 211 nm. Data points represent means ± S.D. from three independent experiments.

more stable than λ-AL light chains (λ-AL-1, 10 ± 1 kJ/mol; λ-MM-2, 14 ± 3 kJ/mol). In summary, MM light chains were marginally more stable than the AL light chains.

Aggregation of Light Chains—LC proteins are deposited in AL patients into amyloid aggregates, which can be stained by amyloidophilic dyes, such as Congo red and ThT. We chose the λ-AL-1 light chain to establish conditions for amyloid formation *in vitro*.

We determined the sequence of the λ-AL-1 LC by MS peptide mapping combined with *de novo* MS sequencing (49). We found 10 point mutations compared with the parent germ line sequence (IGLV1-44*01; IGLC-3*03) (Fig. 4*A*). All mutations are in the V_L domain. Four mutations are concentrated in CDR3 (complementarity-determining region 3). We analyzed the amyloidogenicity of the λ-AL-1 LC using the WALTZ algorithm (50). WALTZ predicted two amyloidogenic regions in the V_L domain of the germ line parent at aa 32–38 and aa 45–51, respectively. Interestingly, mutations S36G and Q44H of the λ-AL-1 light chain flank the first amyloidogenic region. Surprisingly, mutations I54M and N65D in λ-AL-1 removed the amyloidogenicity in the second region. The analysis suggests that the relation between point mutations in clonal LC and amyloid formation is complex. The accumulation of amyloid-promoting mutations is probably not the only factor that determines amyloid formation *in vivo*.

We incubated λ-AL-1 LC for 1 day under permanent shaking in 25 mM sodium phosphate (pH 7.2), 120 mM NaCl at 37 °C. The light chain remained soluble under non-reducing conditions. In contrast, it formed large aggregates when incubated under reducing conditions (8 mM DTT). In native PAGE, we observed LC aggregates (>720 kDa) and high molecular weight (HMW) aggregates incapable of migrating into the gel after 1

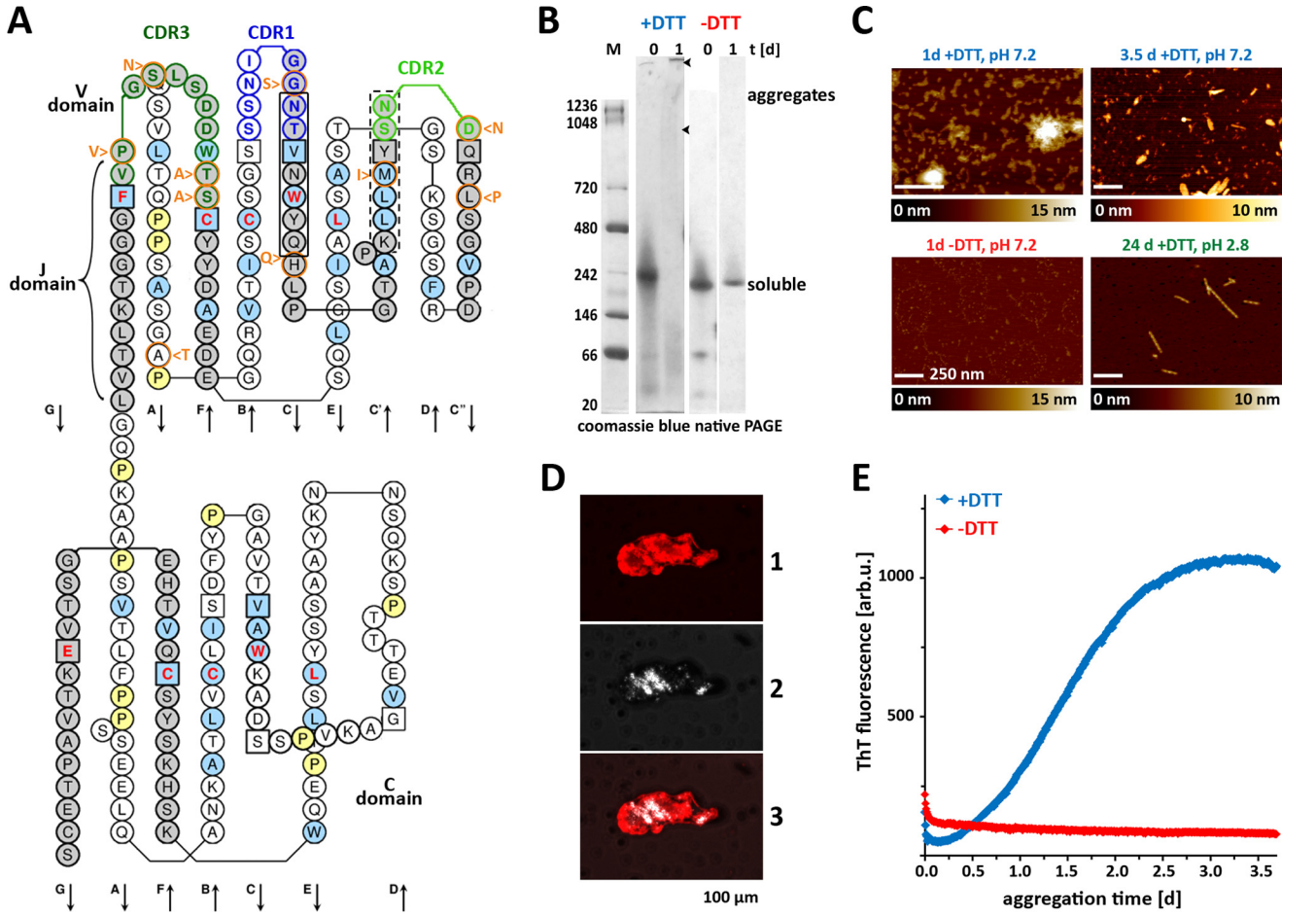

FIGURE 4. **Ig light chain λ-AL-1 aggregated under reducing conditions.** *A*, two-layer Collier de Perles representation of the λ-AL-1 sequence. *Squares*, limits of complementarity-determining regions. Amino acids with *red letters* indicate highly conserved position. Mutations from the germ line parent domain are marked with *orange circles*, and the parent amino acid is shown *beside* each mutation. *B*, native PAGE shows formation of large (>720 kDa) and high molecular weight aggregates incapable of migrating into gel (*arrows*) after incubation of LC (20 μM) for 1 day at 37 °C, in NaP_2 buffer containing DTT (8 mM). *C*, AFM imaging of LC aggregates after 1- and 21-day incubation under neutral or acidic conditions. *D*, λ-AL-1 light chain aggregated for 1 week, stained with Congo red, and imaged by fluorescence (*1*), birefringence (*2*), and overlay (*3*). *E*, ThT-positive aggregates formed only in the presence of DTT (100 mM).

day of incubation (Fig. 4*B*). AFM imaging confirmed that large aggregates were formed in the presence of DTT, whereas in the absence of DTT, no aggregates were visible (Fig. 4*C*). The λ-AL-1 LC formed a mixture of amorphous and fibril-like structures at neutral pH (Fig. 4*C*). These aggregates bound the amyloidophilic dyes ThT and Congo red and displayed Congo red fluorescence and birefringence (Fig. 4, *D* and *E*). Aggregation kinetics followed a sigmoidal time course that is typical for amyloid formation (Fig. 4*E*). We analyzed the aggregation of all nine LC under the same conditions. AL LC formed aggregates with fibrillar substructure at neutral pH, whereas aggregate morphologies of MM LC were diverse. All light chains formed typical amyloid fibrils when incubated at pH 2.8 (Fig. 4*C* and supplemental Fig. 2), displayed SDS resistance (Fig. 5), and bound ThT (Fig. 6). Hence, light chains isolated from patients' urine formed aggregates with amyloid characteristics under reducing conditions.

Characterization of Light Chain Aggregates by Native PAGE and SDS-PAGE—Resistance to denaturation by SDS is a characteristic property of amyloid. We monitored aggregation of light chains over 3 weeks to test whether aggregates would acquire resistance to denaturation in SDS. Samples were frozen after 0, 0.2, 1, 2, 5, 7, 14, and 21 days and stored at −80 °C for further analysis. All nine LC proteins formed large aggregates within 1 day when analyzed by native PAGE (Fig. 5*A*). However, at this time point, LC aggregates were still disaggregated into monomers by 2% LDS at room temperature (semidenaturing conditions). Light chains formed aggregates that were resistant to denaturation at room temperature within 5–7 days (Fig. 5*B*). All nine LC samples displayed similar aggregation kinetics, although MM light chains rapidly formed very large SDS-resistant aggregates that did not enter the gel. In contrast, LC from AL patients produced aggregates that ran as dimers or oligomers (Fig. 5*B*), which may reflect differences in the aggregation mechanism.

To analyze differences in aggregate stability, we denatured LC samples by boiling in 2% LDS after a 21-day incubation. Under these denaturing conditions, LC aggregates dissociated into discrete ladders of monomeric, dimeric, and higher multimeric species (Figs. 5*C* (*top*) and 8). However, a substantial fraction of MM LC remained in the form of HMW aggregates that did not enter the gel. We then performed an ultracentrifugation experiment for 30 min at 200,000 × *g* to test whether SDS-resistant oligomers were the result of a disaggregation of

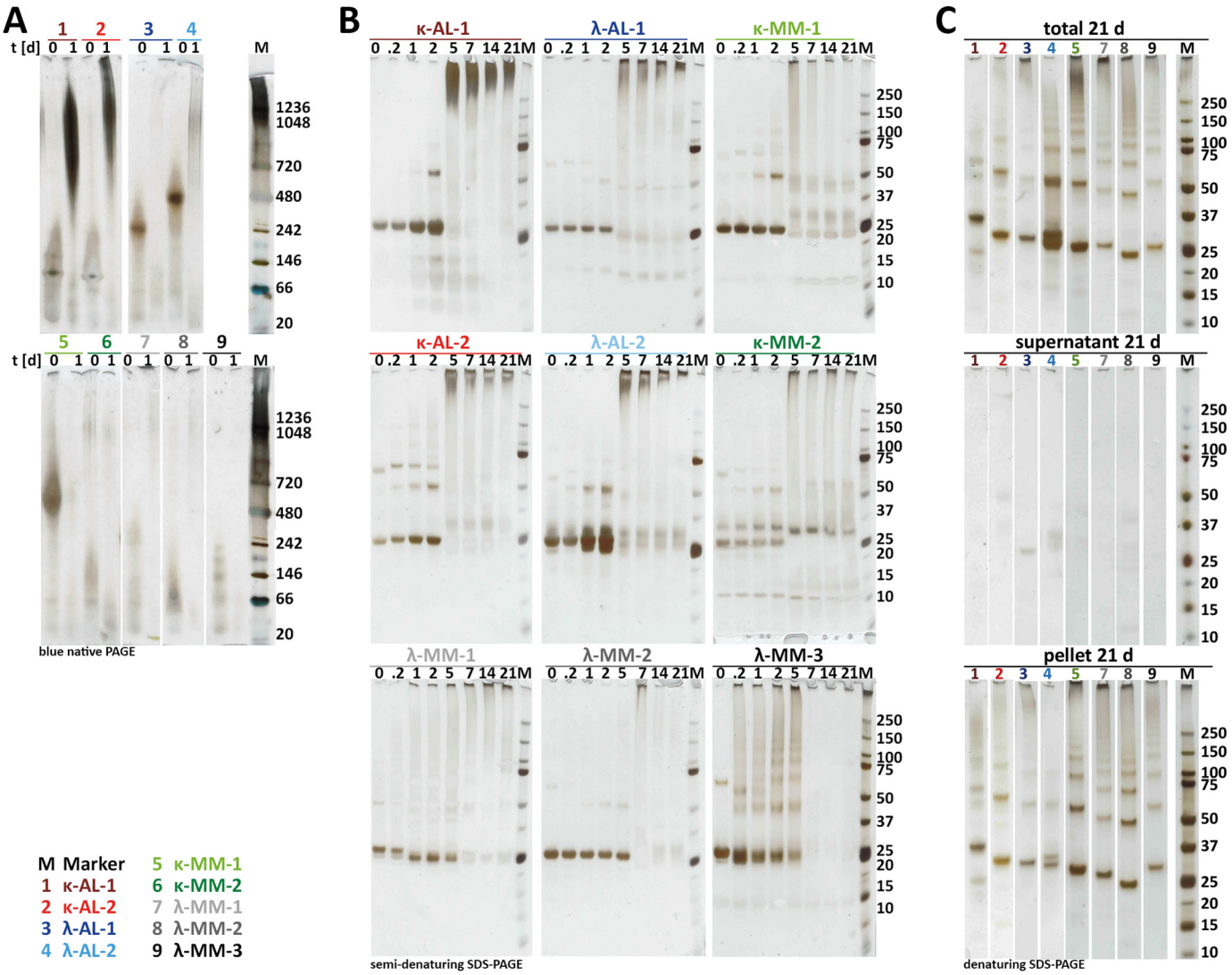

FIGURE 5. *A*, native PAGE of LC aggregated for 1 day. LC proteins formed large aggregates (>720 kDa) and HMW aggregates that were unable to migrate into gels. AL light chains produced mainly large aggregates, and MM samples produced mainly HMW aggregates. *B*, semi-native SDS-PAGE (no DTT, no heat) of LC aggregates formed in long term aggregation assays for 21 days. *C*, ultracentrifugation experiment of 21-day aggregates observed via denaturing SDS-PAGE (DTT, heating to 95 °C). Aggregates from all LC samples dissociated into distinct ladder-like monomeric, dimeric, and multimeric species and residual HMW aggregates (*top*). These species are not soluble protein (*middle*) but insoluble aggregates sensitive to denaturing conditions (*bottom*).

larger aggregates. Supernatants and washed pellets were denatured by boiling in 2% LDS and analyzed by denaturing SDS-PAGE (Fig. 5*C*). All LC protein was pelleted by ultracentrifugation, and no oligomers were visible in the supernatant fraction. This indicates that oligomeric species in SDS-PAGE resulted from partial denaturation of high molecular weight aggregates (Fig. 5*C*).

Aggregation Kinetics of Light Chains—We recorded aggregation kinetics of light chains by ThT fluorescence and by light scattering. Ig light chains formed ThT-positive aggregates at neutral pH under reducing conditions, which could be also observed turbidimetrically (Fig. 6*A*). We observed two types of aggregation kinetics that are represented by the four light chains shown in Fig. 6*A*. In most light chains, ThT aggregation kinetics showed a biphasic behavior with a very rapid initial rise in ThT fluorescence, as exemplified by LC κ-AL-1 and λ-MM-1 (Fig. 6, *A* and *B*, and supplemental Fig. 3, *A* and *B*). This rapid first phase of aggregation was invisible to turbidity measurements. This suggests that it corresponded to the formation of small oligomeric species (Fig. 6*A*). In contrast, the second phase, which was observable in both ThT and light scattering, corresponded to the formation of larger aggregates. However, the relative ThT fluorescence amplitudes of the first and second aggregation phases varied. Light chains λ-AL-1 and κ-MM-1 lacked detectable first aggregation phases.

We tested whether human serum albumin (HSA) had any influence on ThT kinetics of LC proteins by supplementing κ-AL-1 LC aggregation assays with HSA (supplemental Fig. 3 *C*). We found no effect of albumin on the first aggregation phase and a weak delay of the second aggregation phase at 10% of the LC concentration. This albumin concentration was higher than the HSA present in any of our purified LC samples. Therefore, we conclude that albumin had little or no effect on the LC aggregation kinetics under the conditions of our assay.

We could fit aggregation data to two sigmoid growth terms that corresponded to fast oligomer formation and to slower

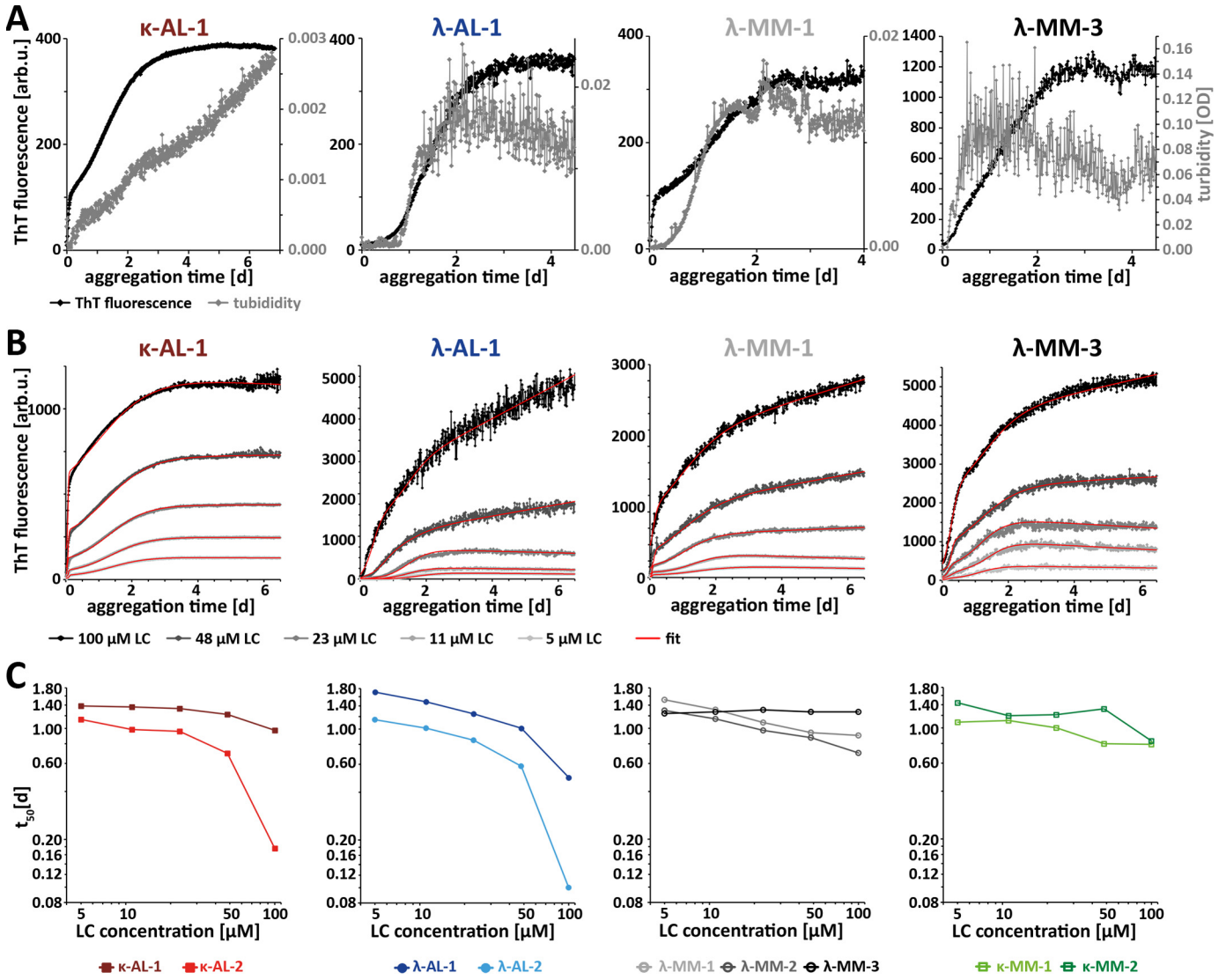

FIGURE 6. *A*, aggregation kinetics measured by ThT fluorescence and turbidity (560 nm) of selected LC samples. *B*, ThT aggregation kinetics at different LC protein concentrations. Samples show biphasic aggregation kinetics that were fitted with two Boltzmann growth terms (*red*). *C*, concentration dependence of the second Boltzmann time constant (t_2) for all LC samples plotted on a logarithmic scale.

fibril formation (Fig. 6*B*). We performed concentration-dependent aggregation assays between 5 and 100 μM initial LC concentration (Fig. 6*B* and supplemental Fig. 3*A*) and determined time constants for both phases of the aggregation kinetics (Fig. 6*C* and supplemental Fig. 3*B*). The second phase of aggregation kinetics depended on protein concentration, whereas the first phase was largely independent of LC concentration. This suggests that a structural transition rather than an assembly step was rate-limiting in the first phase of the aggregation kinetics. We found that the first phase of aggregation accelerated with increasing concentration of DTT (supplemental Fig. 3*D*). These data strongly suggest that oligomer formation was initiated by the reduction of disulfide bonds.

We plotted the time constants (t_{50}) of the second aggregation step logarithmically as a function of LC concentration to analyze the underlying aggregation mechanism (51). All proteins displayed very weak concentration dependences with slopes m between −0.15 and −0.25 at low protein concentrations. Strikingly, concentration dependence of MM LC was weak ($m <$ −0.2) in the whole concentration range probed in our experiment. In contrast, the concentration dependence of most AL LC curved from a flat slope at low concentrations to a slope of ~−0.5 at higher protein concentrations.

Concentration dependences at low LC concentrations are much smaller than what would be predicted for a nucleated polymerization mechanism, for which the concentration dependence of ln t_{50} scales with the nucleus size n as $m = -(n + 1)/2$ (52). A slope of $m = -0.5$ is expected for aggregation that is dominated by secondary nucleation or by prion-like replication of amyloid fibrils (51). Therefore, our data suggest that fibril formation is dominated by unimolecular processes at low LC concentrations. A plausible explanation would be that a conformational conversion step of the LC limits the formation of amyloid fibrils. However, the aggregation of AL LC at higher concentration is dominated by protein assembly. Our data would be compatible with a mechanism that is limited by dimer formation or dominated by secondary processes (51). In contrast, conformational change remained dominant in MM LC under

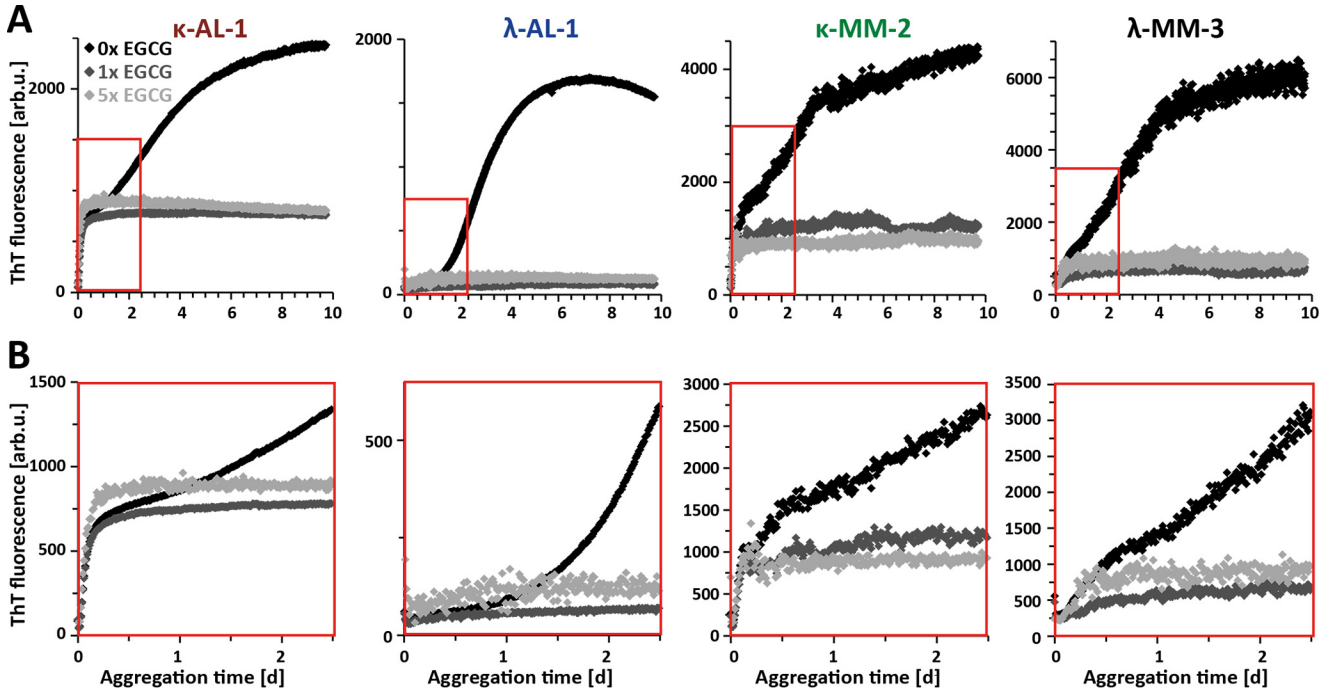

FIGURE 7. *A*, ThT kinetics in the absence (*0*×) of EGCG, with equimolar (*1*×) and 5-fold molar excess of EGCG (*5*×) in relation to LC concentration. EGCG prevented formation of ThT-positive species in the second aggregation phase. *B*, magnification of the first 2.5 days of aggregation.

all conditions. Therefore, our kinetic data suggest that the difference in LC from patients with an AL diagnosis and those from MM patients may lie in the ease with which the LC converts into an amyloid-competent conformation.

The Effect of Epigallocatechin-3-gallate on Light Chain Aggregation—Having established the aggregation characteristics of our light chain proteins, we then analyzed the influence of EGCG on aggregate formation. We incubated Ig light chains under the same conditions as before in presence of equimolar (*1*×) or 5-fold excess (*5*×) of EGCG (Fig. 7, *A* and *B*). In all cases, EGCG completely prevented the second aggregation step but did not affect the first step in ThT kinetics (Fig. 7, *A* and *B*, and supplemental Fig. 4*A*). Correspondingly, the addition of EGCG to the LC sample after the first aggregation step ($t = 4$ h) had the same effect on ThT fluorescence as the addition at $t =$ 0 h (supplemental Fig. 4*B*).

AFM imaging showed that EGCG did not prevent aggregate formation. LC formed aggregates of varied morphologies in the presence of EGCG (supplemental Fig. 2). We therefore tested whether EGCG had changed aggregate stabilities. We and others had previously observed that EGCG can induce the formation of SDS-stable aggregates of other amyloidogenic proteins (31, 53–56). HMW aggregates formed in the absence of EGCG were broken down by boiling in LDS (Fig. 8). Although EGCG had little effect on LC aggregate sizes analyzed by native and semidenaturing PAGE (data not shown), it induced the formation of SDS-stable aggregates (Fig. 8). These SDS-stable aggregates increased in size with prolonged incubation times, whereas LC aggregates remained labile to denaturation in the absence of EGCG.

The data from SDS-PAGE suggest that EGCG induced the formation of insoluble, SDS-resistant aggregates. We tested by ultracentrifugation whether LC treated with EGCG did indeed become insoluble. Aggregates formed in the presence of EGCG after 21 days of incubation were pelleted by ultracentrifugation and analyzed by denaturing SDS-PAGE (Fig. 9). As expected, the aggregates formed in the presence of EGCG were insoluble and pelleted nearly completely.

Therefore, we conclude that EGCG had a similar effect on all nine examined light chains independently of the LC isotype and sequence and the originating disease. EGCG did not prevent the aggregation of the light chains. Rather, it induced their aggregation into SDS-resistant structures. While doing so, EGCG did not fundamentally alter aggregation kinetics of the nine LC relative to each other. LC proteins that rapidly formed HMW aggregates also more rapidly formed SDS-stable aggregates in the presence of EGCG and vice versa.

Discussion

Inhibition of amyloid deposition is emerging as a potential secondary treatment option in AL amyloidosis. Compounds like EGCG can inhibit amyloid formation in a wide variety of misfolded proteins *in vitro* and in animal models (57). Preliminary evidence suggests that EGCG may counteract amyloid deposition in AL patients and improve their prognosis (34, 35, 58). However, the fact that light chains are uniquely different from patient to patient poses specific challenges to the study and to the treatment of AL amyloid deposition.

A number of studies have scrutinized the factors governing LC amyloid formation, most of which have been performed on recombinant variable domains from five different LC proteins: Wil and Jto (18, 19), AL-09 and AL-103 (20–24), and SMA (25, 26). Studies on V_L domains (18, 59–61) found that their amyloidogenicity roughly correlated with their thermodynamic stability. More recent studies have painted a more differentiated picture. Mutations that alter the interface in AL-LC dimers may

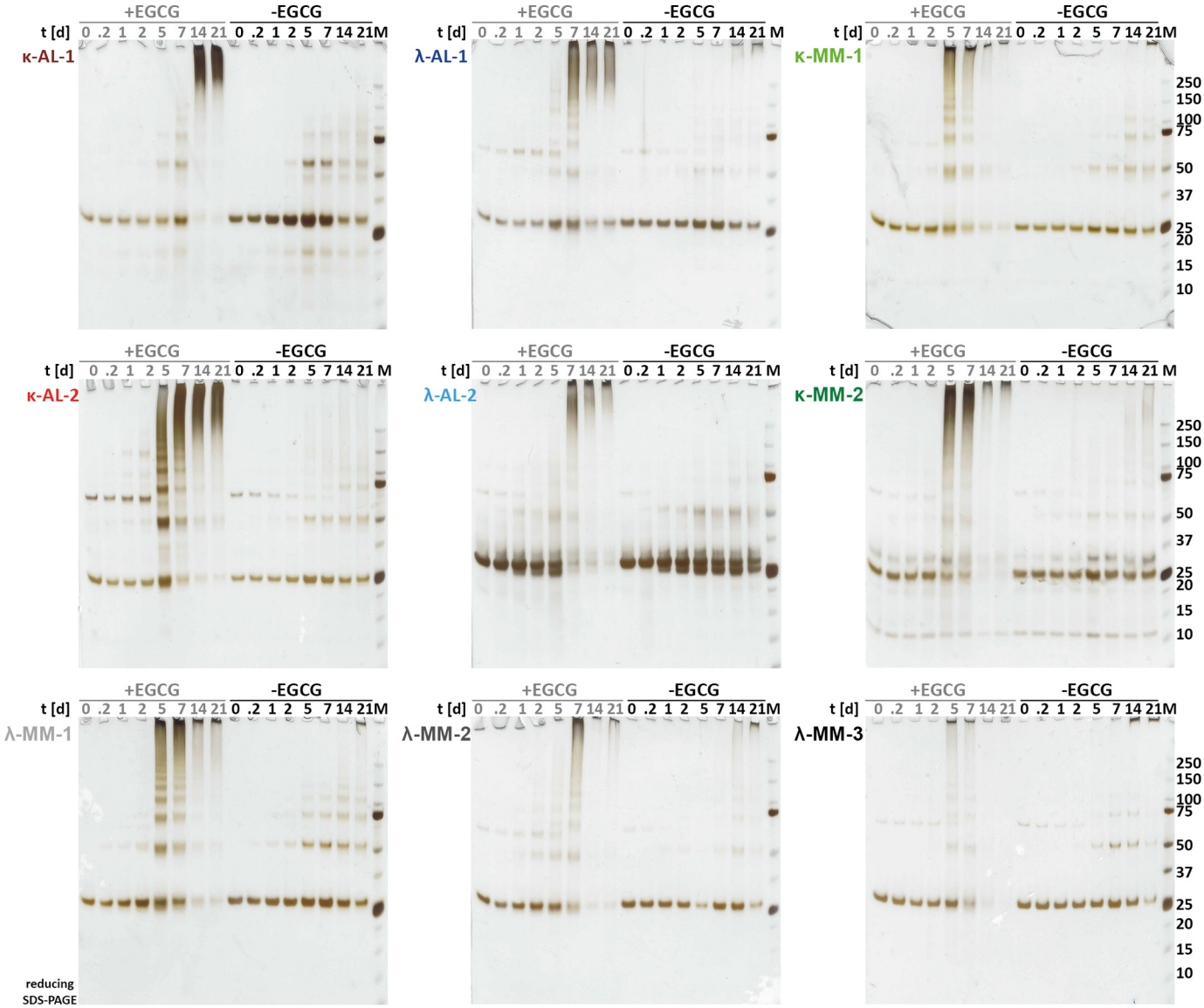

FIGURE 8. **Denaturing SDS-PAGE (DTT, heating to 95 °C) of time points from aggregation assay over 21 days in the presence and absence of equimolar EGCG.** Aggregates of all LC samples were resistant to denaturation only when formed in the presence of EGCG.

alter amyloid formation without altering V_L monomer stability (44, 62).

We have generated detailed sequence information for one of our LC proteins (λ-AL-1) and found 10 substitutions from the germ line parent in the V_L domain but no mutations in the C_L domain. Half of the point mutations in this protein affected regions that are predicted to be amyloidogenic. Interestingly, these mutations did not uniformly increase amyloid propensity. Rather, two mutations flanked region 1 (aa 37–43), and two others strongly reduced the amyloid propensity of region 2 (aa 45–51). At the same time, we have no evidence that the mutations lowered the thermodynamic stability of the LC, because stabilities of all λ-LC were very similar to each other (Fig. 3*F*). This finding supports the hypothesis that mutations in AL LC alter the folding/unfolding pathway rather than destabilize global LC structure. Two mutations (T14A and Q44H) lie at or near the interface between the V_L and C_L domains, and five mutations lie at the LC dimer interface, suggesting that they may alter interdomain contacts. A future full analysis of all nine LC sequences will allow us to assess whether these structural features are unique to λ-AL-1 or whether they are common to amyloid-forming LC proteins.

The significance of full-length LC for amyloid formation was only recently addressed (27–30). These studies find that interactions between the constant and variable domain of LC alter the unfolding/folding pathways and that the unfolding of native state LC is a complex, often irreversible, process. The independent unfolding of the two protein domains fails to explain the observed unfolding dynamics (28, 29, 63). Furthermore, thermodynamic instability is not sufficient for amyloid formation, suggesting the importance of kinetic factors (27, 30). All studies suggest that the enhanced aggregation of the full-length protein results not only from the combined aggregating propensities of its variable and constant domain but also from the intramolecular interactions between these regions.

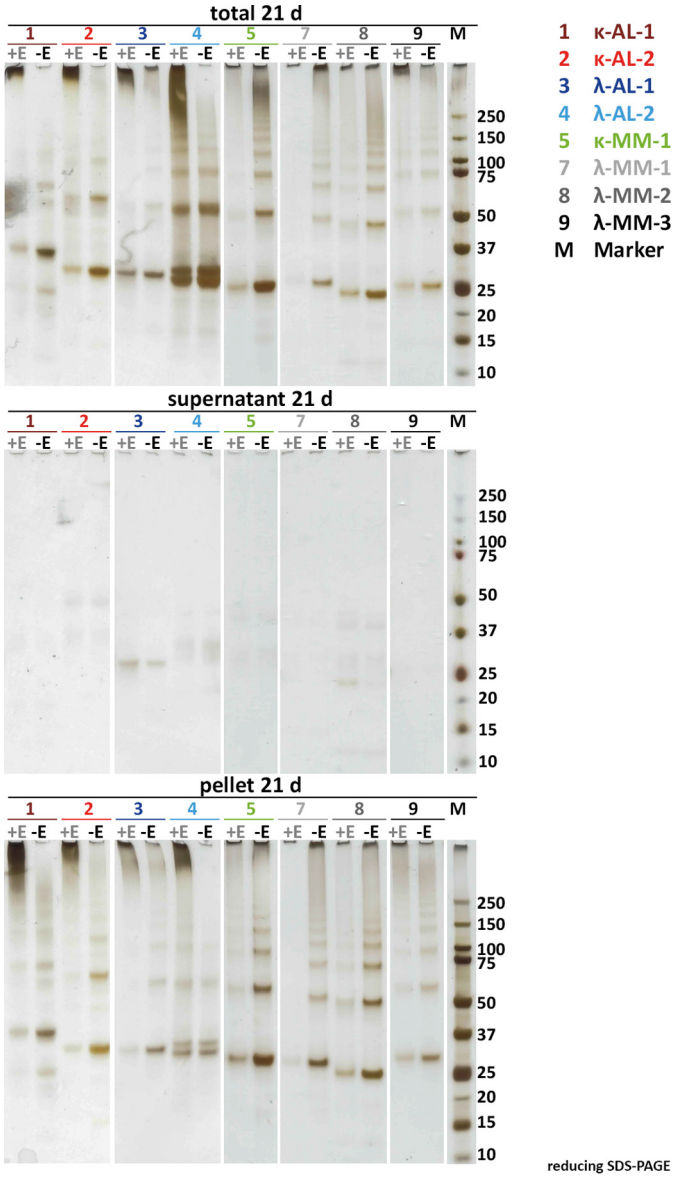

FIGURE 9. **Ultracentrifugation experiment at the 21-day aggregation time point with and without EGCG.** LC proteins became insoluble both in the presence and in the absence of EGCG. Gels show equivalent amounts of total protein before ultracentrifugation (*top*), protein in the soluble fractions (*middle*), and protein in the insoluble fractions (*bottom*).

Our study supports the view that full-length LC differ not only in stability but also in reversibility of unfolding, suggesting different unfolding/folding pathways. Whereas the denaturation of most LC was reversible, all λ-MM LC denatured irreversibly after heating. We found that κ- and λ-isotype LC had different stabilities in thermal denaturation, with an average T_m of 53 ± 5 and 59 ± 2 °C, respectively, which corresponds to previously published data (28, 30, 44, 64). We did not find strong systematic differences in stability between AL- and MM-LC. MM-LC had, on average, slightly higher unfolding energies than AL-LC. We also observed slightly higher melting points of λ-MM-LC compared with λ-AL-LC from thermal denaturation, which would correspond to the results from isolated V_L domains (18). In general, our data support the model that amyloid propensity is unique to each LC and does not correlate strongly with thermodynamic stability.

Our study also supports data from isolated VL domains, which suggest that disruption of intermolecular disulfide bonds in LC dimers is a prerequisite of amyloid formation (61, 65). This model is also supported by data from a recent drug screen (66). We found that ~50% of LC in urine existed as disulfide-cross-linked dimers, and all LC existed as di- or multimers under native conditions. Efficient amyloid formation under our experimental conditions required the reduction of intermolecular disulfide bonds. Although disulfide bonds were not reduced in other aggregation studies of LC, these studies employed temperatures near the melting point, low pH, and/or very long incubation times to achieve amyloid formation (27, 30). These results suggest that the stability of folded light chains needs to be compromised for amyloid formation. Although analysis of LC from serum by immunoaffinity LC-MS/MS (67) did not resolve to what degree disulfide-linked dimers are present in the serum of patients, our data suggest that a reducing milieu may initiate amyloid formation *in vivo*. Specifically, aggregation was initiated by the reduction of interchain and intermolecular disulfide bonds. In contrast, intradomain disulfide bond were only cleaved under denaturing conditions but stayed intact under native conditions (43). We found that LC were present in oligomeric form in the urine samples. After reduction of intermolecular disulfide bonds, LC ran as monomers in native PAGE, suggesting that disulfide bonds stabilized LC oligomers.

Both the V_L and C_L domains of LC display complex unfolding mechanisms (68, 69). Our data suggest that reduction of intermolecular disulfide bonds did not alter LC domain structure. However, it made protein surfaces accessible that would otherwise be obstructed in the di- or oligomer. Notably, the amyloidogenic regions of the λ-AL-1 LC map to a single defined region on the surface of the V_L domain (Fig. 4*A*). We hypothesize that monomerization enabled LC to enter a partial unfolding route that allows amyloid formation. This model would explain the two-phase aggregation kinetics with a first fast DTT-dependent oligomeric phase and a second phase where cross-β-sheet structures are formed, which were inhibited by EGCG.

V_L domains of light chains form amyloid fibrils under acidic and neutral conditions (18, 70). Meshlike structures were observed after prolonged incubation of recombinant full-length LC at neutral pH under permanent shaking (30). We found that patient-derived LC from AL patients formed similar fibril cluster structures after 3 weeks of constant agitation (Fig. 4*C* and supplemental Fig. 2). These aggregates bound the amyloidophilic dyes ThT and Congo red and showed Congo red birefringence, suggesting that they contained cross-β-sheet amyloid structures.

Aggregation studies of recombinant V_L and LC find sigmoidal aggregation kinetics typical of amyloid formation. Our study found that native reducing conditions rapidly induce amyloid formation of authentic LC at physiological pH, salt, and temperature. Kinetics could be described by a common two-phase aggregation mechanism. The first phase was independent of the LC concentration and varied in relative ThT fluorescence amplitude. The second phase displayed sigmoid kinetics. Two-phase aggregation kinetics have been observed in

Aβ aggregation, where oligomers formed in the first aggregation phase (71, 72). Non-amyloid aggregation processes with oligomer formation also present similar kinetics (73).

The first phase of LC aggregation kinetics depended on the DTT concentration but not on LC concentration, suggesting that reduction of disulfide bonds is the rate-limiting process resulting in the formation of LC oligomers. The second aggregation phase was concentration-dependent for most light chains. However, analysis of the reaction order in a double logarithmic plot as a function of LC concentration suggests that conformational change rather than aggregate assembly or propagation may be limiting amyloid formation at low LC concentrations.

At high protein concentrations, aggregation of light chains from AL patients switched from kinetics that were dominated by structural conversion to kinetics that are compatible with a nucleated polymerization mechanism. These data suggest that AL and MM LC may differ in the kinetics of early conformational change, which makes the protein competent for amyloid formation. Our data also suggest that molecular AL and MM pathologies could exist on a continuum and that additional factors, such as protein homeostasis, may determine the ultimate fate of LC *in vivo* (74).

Although our use of authentic LC from urine avoided potential bias from lack of posttranslational modifications, it may have introduced a degree of sampling bias. We found that the albumin in the urine of AL patients with albuminuria tightly bound to LC and co-eluted with the light chains in size exclusion chromatography (data not shown). It was reported that albumin can bind proteins covalently via disulfide bond formation (75, 76), but our biochemical analysis under non-reducing conditions indicated a non-covalent binding mode between the two proteins (Fig. 1*B*). The strong interaction between albumin and LC made it impossible to purify LC from the urine of patients with albuminuria under native conditions. We therefore excluded urine samples with high albumin content from the analysis.

We performed patient selection, sample purification, and biophysical studies blind to the detailed clinical diagnosis. After unblinding the patient samples, we found that our selection criteria (high LC, low albumin) directed AL patient selection toward AL deposits in soft tissue and gastrointestinal tract (Table 1). As a consequence, the underlying plasma cell clone of all of these AL patients had expanded to symptomatic MM with bone lesions. The fact that our experimental approach selected for AL patients with a "weak" amyloid deposition phenotype may account for the modest differences in aggregation kinetics between AL and MM patient samples. It is reasonable to assume that LC proteins from AL patients with strong heart or kidney pathology would display a stronger difference in aggregation kinetics from MM LC, as had been observed in previous studies (27).

Since its discovery as an anti-amyloid agent, the mechanism of EGCG has been studied in a number of proteins. EGCG prevented fibril formation in Aβ and α-Syn aggregation (31, 32, 77), delayed aggregation kinetics (31, 32, 55, 78–81), and redirected misfolded proteins into SDS-stable aggregates (31, 32, 55, 56, 79). Treatment with EGCG disaggregated preformed amyloid fibrils by remodeling them into large amorphous aggregates (31, 56, 77) and reduced amyloid seeding competence (31, 32, 56, 82, 83).

We have studied the effect of EGCG on nine authentic full-length LC proteins and found that EGCG had a generic, sequence-independent effect on light chain aggregation. It prevented the second aggregation phase and induced the formation of SDS-stable aggregates. These observations are similar to those in Aβ and α-Syn aggregation, suggesting a similar mechanism, in which EGCG preferentially interacts with aggregation intermediates of LC and inactivates them via off-pathway aggregate formation. This is seemingly in contrast to recent data finding that EGCG binds to the V_L domain of LC with 1:1 stoichiometry and a dissociation constant of ~75 μM (80).

However, binding studies on Aβ revealed that EGCG can interact both with the monomeric peptide (84, 85) and with amyloid fibrils (56, 82). When systematically reviewing EGCG mechanisms in various proteins, we found that EGCG binding to aggregation intermediates may inhibit amyloid formation very effectively in cases where these species are rate-limiting to amyloid formation (57). In other cases, amyloid formation is dominated by a structural transition or dissociation of the native protein. Here, EGCG may bind to native proteins and have less of an effect on kinetics but may nevertheless divert the protein into stable non-amyloid aggregates (57).

We find that EGCG effectively inhibits amyloid formation of a variety of light chains *in vitro*. This suggests that treatment with anti-amyloid drugs that either stabilize the native LC dimer or inhibit amyloid formation may be a promising supplemental therapeutic strategy to ameliorate the amyloid pathology in AL patients. It would therefore be valuable to assess the potential of drugs, such as EGCG, methylene blue, and Orcein/O4, which have proven effective in inhibiting amyloid formation in other disease-related proteins, for the treatment of AL amyloidosis (32, 66, 86).

Experimental Procedures

Diagnosis and Patient Selection for This Study—Patients were diagnosed for monoclonal gammopathy by FLC from serum and immunofixation electrophoresis from serum as well as from urine (87). The diagnosis of AL amyloidosis was established via Congo red staining of fat aspirates and/or tissue biopsies (6) at the Amyloidosis Center Heidelberg according to established clinical protocols and in compliance with the ethical guidelines for treatment and patient consent. Patients were selected who presented with >265 mg/24 h clonal light chain in urine but without significant albuminuria (<6% albumin). 24-h urine samples were collected, and aliquots of 4 × 15 ml were frozen afterward at −20 °C for storage in the Heidelberg Amyloidosis Center biobank. Nine immunoglobulin light chains were purified from patient urine and subsequently analyzed: 2× κ-AL, 2× λ-AL, 2× κ-MM, and 3× λ-MM (Table 1). The deposition patterns in the AL patients were blinded until after all experimental data were acquired.

Light Chain Protein Purification from Human Urine—Immunoglobulin light chains were isolated from patients suffering from AL or MM as follows. Particulate matter was removed from 20–40 ml of patient urine by centrifugation for 15 min at

4,500 × *g* at 4 °C, followed by sequential filtration through first a 5-μm and second a 0.22-μm syringe membrane filter (Millipore). Afterward, the protein was concentrated in ultrafiltration units (Amicon Ultra 15) to 0.5 ml and buffer-exchanged in the same by six sequential dilution and reconcentration steps in 50 mM sodium phosphate (NaP) buffer, pH 7.2 (6 × 15 ml).

Total protein concentrations were determined via BCA assay (Pierce). The albumin content was estimated densitometrically from silver-stained SDS-PAGE *versus* an HSA standard. Samples were adjusted to final LC concentrations of 1 mM, flash-frozen, and stored at −80 °C.

LC-MS/MS-based Sequencing—Lyophilized λ-AL-1 sample (5 μg) was reconstituted with 20 μl of ultrapure water. Gel bands from reducing SDS-PAGE were excised, destained, reduced, and alkylated as described previously (49). The protein was digested in-gel at 37 °C overnight with 0.025 μg/μl trypsin (Promega) or chymotrypsin (bovine; Promega) and for 3 h at room temperature with 0.025 μg/μl GluC (*Staphylococcus aureus*, Roche Applied Science) in 20 mM Tris, pH 8.2, 0.0002% Zwittergent 3-16. Peptide extraction was performed in two steps with 25 μl of 2% trifluoroacetic acid and 50 μl of acetonitrile. Samples were lyophilized and stored at −80 °C before MS analysis.

Nano-LC-electrospray ionization-MS/MS measurements were performed as described previously (49) with an Orbitrap Elite detector and the following LC gradient of solvent B: 5 to 45% in 39 min, 45 to 90% in 2 min, 90% for 5 min, 90 to 5% in 2 min. The mass spectrometer performed a full scan MS scan from 340–1,500 *m*/*z*, with a resolution of 140,000, followed by MS/MS scans at a resolution of 17,500. The Top20 $[M + 2H^+]$ 2+, $[M + 3H^+]$ 3+, and $[M + 4H^+]$ 4+ ions were analyzed in a 1.5 *m*/*z* isolation window.

MS data were processed in PEAKS Studio software (Bioinformatics Solutions, Waterloo, Canada). For peptide mapping, a homemade IMGT-derived LC sequence database and the Uniprot human protein database were combined. The IMGT-derived database contained V_L-J_L-C_L transition peptide sequences, and complete V_L and C_L domain sequences. Database searches and *de novo* sequencing were performed assuming cysteine carbamidomethylation as a fixed modification, and methionine oxidations and asparagine/glutamine deamination as variable modifications. Additionally, the PEAKS PTM and the SPIDER search algorithm were used to detect PTMs and mutations. A precursor mass tolerance of 4.5 ppm and a fragment tolerance of 0.02 Da (49) were selected.

Relevant identified peptide sequences were determined by base peak interrogation as described previously (49) and aligned to the IMGT numbering system (16, 17, 45) with the IMGT/DomainGapAlign tool (88). Missing sequence patches were identified via inverse interrogation of the PEAKS results and LC-MS/MS data. The sequence representation shown here was created using the IMGT/Collier de Perles tool (89, 90). Amino acids are numbered according to the IMGT numbering system. Amyloidogenicity of LC sequence was predicted using the WALTZ online tool, as described (50).

Gel Electrophoresis, Western Blotting Analysis, SDS Stability Assays, and Molecular Weight Determination—For SDS-PAGE and blue native PAGE, NuPAGE and NativePAGE precast gel systems (Invitrogen) were used with precast gradient gels (3–12% and 4–12%, respectively). For SDS-PAGE, samples were diluted in LDS sample buffer (Invitrogen) either reduced with DTT (187.5 mM) and heated for 10 min to 95 °C (denaturing conditions) or directly applied to the gel (semidenaturing). Gel bands were visualized either by Coomassie staining (EZ blue) or silver staining (ProteoSilver kit, both from Sigma-Aldrich) according to the manufacturer's protocols with minor changes. In short, the volumes of all kit components were reduced by a factor of 4, whereas the volumes of fixing solution, ethanol, and water washes were reduced by a factor of 2. The gels were stained in single-use plastic dishes, and the incubation with the silver solution was elongated to 15 min, following three short consecutive rinsing steps with ultrapure water.

For Western blotting analysis, proteins were transferred to nitrocellulose membranes. Membranes were blocked for 30 min in 3% milk in PBS and then were either immunostained for λ-isotype LC and HSA or κ-isotype LC and HSA in parallel. As primary antibodies, we used polyclonal goat anti-human Ig λ chain, polyclonal goat anti-human Ig κ chain (both 1:2,000; Millipore, AP506 and AP502), and polyclonal rabbit anti-human HSA (1:2,000; Thermo, R0101-1D). As secondary antibodies IRDye® 800CW donkey anti-goat IgG and LI-COR IRDye® 680RD donkey anti-rabbit IgG were used (both 1:15,000; LI-COR, 926-32214 and 926-68073). All antibodies were diluted in 3% milk in PBS. Secondary antibodies were detected in a fluorescent detection system (LI-COR) at 800-nm (LC) or 700-nm wavelength (HSA). We determined the apparent molecular weight of the light chains compared with a protein marker (Precision Dual Plus, Bio-Rad) from three independent SDS-PAGE samples.

CD Spectroscopy, Thermal and Chemical Denaturation—CD spectroscopy was performed in a JASCO J-810 CD spectrometer. CD spectra were accumulated between 265 and 190 nm with bandwidth 1 nm, response time 8 s, standard sensitivity, data pitch 0.5 nm, scanning speed 50 nm/min, 0.1-cm cell length at 20 °C, and 3 accumulations at a concentration of 10–20 μM LC in NaP buffer. Thermal de- and renaturations were performed in triplicate at a temperature slope of 0.5 °C/min. Spectra before and after denaturation and after renaturation were acquired to test for refolding of the light chains. For thermal denaturation under reducing conditions, LC (200 μM) was reduced with DTT (10 mM) for 2 h at room temperature either in NaP buffer or in 2 M GdnHCl. LC samples were renatured by dilution to 10 μM in NaP.

GdnHCl denaturation was performed in biological triplicates by incubating the samples overnight at the respective concentrations of GdnHCl in NaP buffer before measurement. For renaturation samples, the protein was unfolded overnight at 100 μM LC and 6 M GdnHCl, diluted to 10 μM LC at the desired GdnHCl concentration, and incubated for at least 8 h. For GdnHCl denaturation, three CD spectra with three accumulations were measured between 213 and 211 nm using the spectrometer's interval measurement mode with bandwidth 1 nm, response time 16 s, standard sensitivity, data pitch 0.1 nm, scanning speed 20 nm/min, and 0.1-cm cell length, at a concentration of 10 μM at 20 °C. Protein unfolding curves were deter-

mined at 211 nm. Spectra before and after denaturation and after renaturation were acquired as described above.

Tryptophan Fluorescence Spectroscopy, Guanidine Denaturation—We incubated LC samples overnight in biological triplicates, and Trp fluorescence was recorded between 300 and 470 nm in a spectrofluorimeter (Photon Technology International) at room temperature at 0.5 μM LC in NaP, excitation at 280 nm. Samples for GdnHCl denaturation were prepared as described for CD but in disposable borosilicate glass culture tubes (10 × 75 mm) (Fisher) to avoid the leaching of fluorescent molecules from plastic tubes into the sample.

To calculate the degree of unfolding, we determined the ratio between fluorescence intensities of the emission maximum before denaturation (*e.g.* 339 nm) and after denaturation (*e.g.* 351 nm). Different samples exhibited different peak shifts, which are summarized in Table 2.

Aggregation Assays—Short term aggregation assays were performed with the following parameters: 5–100 μM LC, NaP buffer (pH 7.2), 150 mM sodium chloride, 100 mM DTT, 20 μM ThT, 0.05% sodium azide, with or without EGCG (equimolar, 5× equimolar; Taiyo) in a 100-μl volume in non-binding surface 96-well plates, (Corning, catalog no. 3991). For measurements, we used a Tecan Infinite F200 filter based plate reader, 436/10-nm excitation band pass filter, and 482/25-nm emission filter. Measurements were performed at 37 °C after 5 s of linear shaking with 2.5-mm amplitude in 15-min cycles. For turbidity measurements, absorption was measured at 560 nm. In concentration-dependent aggregation assays, we ran background traces containing the respective albumin concentration and subtracted the albumin signal before analyzing the data further.

Long term aggregation assays were performed in 200-μl 8-tube PCR strips (Simport Scientific, Saint-Mathieu-de-Beloei, Canada) with 20 μM LC, 25 mM sodium phosphate (NaP_2, pH 7.2), 120 mM sodium chloride, 8 mM DTT, 16 μM ThT, 0.05% sodium azide, and 50-μl assay volume. Quadruplicates were incubated with and without 40 μM EGCG for different time periods up to 21 days under permanent shaking with 200 rpm at 37 °C in an incubator shaker (New Brunswick). Samples were stored at −80 °C at each time point, afterward pipetted in non-binding surface 348-well plates (Corning, catalog no. 3544). Absorption and/or ThT fluorescence were measured as described above, including prior shaking. Samples were recovered from 348-well plates for further biochemical analysis. For EGCG stock solutions, EGCG was dissolved and diluted in ultrapure water directly before use.

Ultracentrifugation Assays—Ultracentrifugation assays were performed in a Beckman TL-100 ultracentrifuge, with a TLA-100 fixed angle rotor in thick walled polycarbonate 200-μl tubes (Beckman Coulter) at 75,000 rpm (189,000–245,000 × *g*) and 4 °C. The pellets were washed with 200 μl of NaP buffer, again centrifuged for 30 min, and resuspended in SDS-PAGE LDS sample buffer, 187.5 mM DTT, and boiled for 5 min and analyzed by SDS-PAGE.

Atomic Force Microscopy Imaging—For AFM measurements, 10 μl of 5 μM sample was applied to grade V-1 Mica (catalog no. 01792-AB, Structure Probe, Inc.), followed by six wash steps with 15 μl of ultrapure water. Samples were dried overnight, and AFM images were acquired on a Veeco Dimension 3100 machine with Bruker FESP tips. Scans were accumulated in tapping mode with 512 points/line for 10 × 10- or 3 × 3-μm scan range, with a scan rate of 0.6 Hz.

Congo Red Staining and Imaging—Congo red (50 μM) was added to λ-AL-1 LC (20 μM) that had been aggregated for 1 week under standard conditions. The aggregate solution was pipetted on a coverslip and imaged by fluorescence microscopy and by birefringence in a Zeiss Axio imager at ×5 magnification. Fluorescence was detected at 546 nm excitation and 575–640 nm emission. Birefringence was measured under white light using two polarizers angled at 90°.

Evaluation of Unfolding Data—To determine unfolding energies for light chain proteins by CD and/or fluorescence spectroscopy, different properties had to be evaluated for different samples due to structural characteristics: (*a*) the ellipticity at 211 nm for the fluorescence intensity for samples κ-AL-1, κ-MM-2, and κ-MM-2; (*b*) the fluorescence intensity at 350 nm for the κ-AL-2; and (*c*) the ratio between fluorescence intensities at the lowest and the highest wavelength at the peak maximum observed for the other λ-LC samples. Unfolding curves were calculated from raw data as a function of the GdnHCl concentration by first correcting for pre- and post-transition baseline. Second, we assumed a two-state transition for the unfolding, an equilibrium state at each data point, and a completely folded and unfolded state at the beginning and end GdnHCl concentration, respectively. For each sample, the transition unfolding equilibrium constants K and $\ln K$ were determined as a function of the GdnHCl concentration. The Gibbs free energy (ΔG_0) was determined via linear regression from Equation 1 (91).

$$\ln K = -m' \times c_{\text{denaturant}} + \left(\frac{\Delta G_0}{-RT}\right) \qquad \text{(Eq. 1)}$$

Fitting of ThT Aggregation Curves—Concentration-dependent aggregation data were fitted with a two-phase Boltzmann growth function with a linear correction term (Equation 2). Time constants of Boltzmann growth phases were plotted double logarithmically as functions of initial LC concentration and data points fitted with linear regression.

$$y = A_0 + \frac{(A_1 - A_0)}{1 + \exp^{(t_1 - x)/dx_1}} + \frac{(A_2 - A_1)}{1 + \exp^{(t_2 - x)/dx_2}} + m \times x \qquad \text{(Eq. 2)}$$

Author Contributions—K. A. designed and performed experiments and wrote the manuscript; N. K. performed additional experiments; J. B. provided scientific infrastructure, designed and discussed experiments, and co-wrote the manuscript; E. W. provided scientific infrastructure and discussed experiments. H. R. B. performed MS analysis and discussed LC sequencing data. C. K. provided samples and characterized and diagnosed AL and MM patients. U. H. and S. S. discussed experiments, provided samples, and characterized and diagnosed AL and MM patients. All authors contributed to the editing of the manuscript.

Acknowledgment—We gratefully acknowledge the use of the Nano Research Facility (Washington University, St. Louis, MO).

References

1. Desport, E., Bridoux, F., Sirac, C., Delbes, S., Bender, S., Fernandez, B., Quellard, N., Lacombe, C., Goujon, J. M., Lavergne, D., Abraham, J., Touchard, G., Fermand, J. P., Jaccard, A., and Centre national de référence pour l'amylose AL et les autres maladies par dépôts d'immunoglobulines monoclonales (2012) Al amyloidosis. *Orphanet J. Rare Dis.* **7,** 54
2. Kyle, R. A., Linos, A., Beard, C. M., Linke, R. P., Gertz, M. A., O'Fallon, W. M., and Kurland, L. T. (1992) Incidence and natural history of primary systemic amyloidosis in Olmsted County, Minnesota, 1950 through 1989. *Blood* **79,** 1817–1822
3. Sölling, K. (1976) Polymeric forms of free light chains in serum from normal individuals and from patients with renal diseases. *Scand. J. Clin. Lab. Invest.* **36,** 447–452
4. Teppo, A. M., and Groop, L. (1985) Urinary excretion of plasma proteins in diabetic subjects: increased excretion of κ light chains in diabetic patients with and without proliferative retinopathy. *Diabetes* **34,** 589–594
5. Robinson, E. L., Gowland, E., Ward, I. D., and Scarffe, J. H. (1982) Radioimmunoassay of free light chains of immunoglobulins in urine. *Clin. Chem.* **28,** 2254–2258
6. Klatskin, G. (1969) Nonspecific green birefringence in Congo red-stained tissues. *Am. J. Pathol.* **56,** 1–13
7. Saeed, S. M., and Fine, G. (1967) Thioflavin-T for amyloid detection. *Am. J. Clin. Pathol.* **47,** 588–593
8. Li, C., and Mezzenga, R. (2013) The interplay between carbon nanomaterials and amyloid fibrils in bio-nanotechnology. *Nanoscale* **5,** 6207–6218
9. Li, C., Bolisetty, S., and Mezzenga, R. (2013) Hybrid nanocomposites of gold single-crystal platelets and amyloid fibrils with tunable fluorescence, conductivity, and sensing properties. *Adv. Mater.* **25,** 3694–3700
10. Davies, D. R., Padlan, E. A., and Segal, D. M. (1975) Three-dimensional structure of immunoglobulins. *Annu. Rev. Biochem.* **44,** 639–667
11. Poljak, R. J. (1975) Three-dimensional structure, function and genetic control of immunoglobulins. *Nature* **256,** 373–376
12. Silverton, E. W., Navia, M. A., and Davies, D. R. (1977) Three-dimensional structure of an intact human immunoglobulin. *Proc. Natl. Acad. Sci. U.S.A.* **74,** 5140–5144
13. Amzel, L. M., and Poljak, R. J. (1979) Three-dimensional structure of immunoglobulins. *Annu. Rev. Biochem.* **48,** 961–997
14. Lefranc, M. P. (2003) IMGT, the international ImMunoGeneTics database. *Nucleic Acids Res.* **31,** 307–310
15. Lefranc, M. P. (2004) IMGT-ONTOLOGY and IMGT databases, tools and Web resources for immunogenetics and immunoinformatics. *Mol. Immunol.* **40,** 647–660
16. Lefranc, M. P., Pommié, C., Kaas, Q., Duprat, E., Bosc, N., Guiraudou, D., Jean, C., Ruiz, M., Da Piédade, I., Rouard, M., Foulquier, E., Thouvenin, V., and Lefranc, G. (2005) IMGT unique numbering for immunoglobulin and T cell receptor constant domains and Ig superfamily C-like domains. *Dev. Comp. Immunol.* **29,** 185–203
17. Lefranc, M. P., Pommié, C., Ruiz, M., Giudicelli, V., Foulquier, E., Truong, L., Thouvenin-Contet, V., and Lefranc, G. (2003) IMGT unique numbering for immunoglobulin and T cell receptor variable domains and Ig superfamily V-like domains. *Dev. Comp. Immunol.* **27,** 55–77
18. Wall, J., Schell, M., Murphy, C., Hrncic, R., Stevens, F. J., and Solomon, A. (1999) Thermodynamic instability of human lambda 6 light chains: correlation with fibrillogenicity. *Biochemistry* **38,** 14101–14108
19. Abe, M., Abe, Y., Ohkuri, T., Mishima, T., Monji, A., Kanba, S., and Ueda, T. (2013) Mechanism for retardation of amyloid fibril formation by sugars in Vλ6 protein. *Protein Sci.* **22,** 467–474
20. McLaughlin, R. W., De Stigter, J. K., Sikkink, L. A., Baden, E. M., and Ramirez-Alvarado, M. (2006) The effects of sodium sulfate, glycosaminoglycans, and Congo red on the structure, stability, and amyloid formation of an immunoglobulin light-chain protein. *Protein Sci.* **15,** 1710–1722
21. Martin, D. J., and Ramirez-Alvarado, M. (2010) Comparison of amyloid fibril formation by two closely related immunoglobulin light chain variable domains. *Amyloid* **17,** 129–136
22. Martin, D. J., and Ramirez-Alvarado, M. (2011) Glycosaminoglycans promote fibril formation by amyloidogenic immunoglobulin light chains through a transient interaction. *Biophys. Chem.* **158,** 81–89
23. DiCostanzo, A. C., Thompson, J. R., Peterson, F. C., Volkman, B. F., and Ramirez-Alvarado, M. (2012) Tyrosine residues mediate fibril formation in a dynamic light chain dimer interface. *J. Biol. Chem.* **287,** 27997–28006
24. Poshusta, T. L., Katoh, N., Gertz, M. A., Dispenzieri, A., and Ramirez-Alvarado, M. (2013) Thermal stability threshold for amyloid formation in light chain amyloidosis. *Int. J. Mol. Sci.* **14,** 22604–22617
25. Khurana, R., Gillespie, J. R., Talapatra, A., Minert, L. J., Ionescu-Zanetti, C., Millett, I., and Fink, A. L. (2001) Partially folded intermediates as critical precursors of light chain amyloid fibrils and amorphous aggregates. *Biochemistry* **40,** 3525–3535
26. Stevens, P. W., Raffen, R., Hanson, D. K., Deng, Y. L., Berrios-Hammond, M., Westholm, F. A., Murphy, C., Eulitz, M., Wetzel, R., and Solomon, A. (1995) Recombinant immunoglobulin variable domains generated from synthetic genes provide a system for *in vitro* characterization of light-chain amyloid proteins. *Protein Sci.* **4,** 421–432
27. Sikkink, L. A., and Ramirez-Alvarado, M. (2008) Biochemical and aggregation analysis of Bence Jones proteins from different light chain diseases. *Amyloid* **15,** 29–39
28. Klimtchuk, E. S., Gursky, O., Patel, R. S., Laporte, K. L., Connors, L. H., Skinner, M., and Seldin, D. C. (2010) The critical role of the constant region in thermal stability and aggregation of amyloidogenic immunoglobulin light chain. *Biochemistry* **49,** 9848–9857
29. Davern, S., Murphy, C. L., O'Neill, H., Wall, J. S., Weiss, D. T., and Solomon, A. (2011) Effect of lysine modification on the stability and cellular binding of human amyloidogenic light chains. *Biochim. Biophys. Acta* **1812,** 32–40
30. Blancas-Mejía, L. M., Horn, T. J., Marin-Argany, M., Auton, M., Tischer, A., and Ramirez-Alvarado, M. (2015) Thermodynamic and fibril formation studies of full length immunoglobulin light chain AL-09 and its germline protein using scan rate dependent thermal unfolding. *Biophys. Chem.* **207,** 13–20
31. Bieschke, J., Russ, J., Friedrich, R. P., Ehrnhoefer, D. E., Wobst, H., Neugebauer, K., and Wanker, E. E. (2010) EGCG remodels mature α-synuclein and amyloid-β fibrils and reduces cellular toxicity. *Proc. Natl. Acad. Sci. U.S.A.* **107,** 7710–7715
32. Ehrnhoefer, D. E., Bieschke, J., Boeddrich, A., Herbst, M., Masino, L., Lurz, R., Engemann, S., Pastore, A., and Wanker, E. E. (2008) EGCG redirects amyloidogenic polypeptides into unstructured, off-pathway oligomers. *Nat. Struct. Mol. Biol.* **15,** 558–566
33. Ehrnhoefer, D. E., Duennwald, M., Markovic, P., Wacker, J. L., Engemann, S., Roark, M., Legleiter, J., Marsh, J. L., Thompson, L. M., Lindquist, S., Muchowski, P. J., and Wanker, E. E. (2006) Green tea (−)-epigallocatechin-gallate modulates early events in huntingtin misfolding and reduces toxicity in Huntington's disease models. *Hum. Mol. Genet.* **15,** 2743–2751
34. Hunstein, W. (2007) Epigallocathechin-3-gallate in AL amyloidosis: a new therapeutic option? *Blood* **110,** 2216
35. Mereles, D., Buss, S. J., Hardt, S. E., Hunstein, W., and Katus, H. A. (2010) Effects of the main green tea polyphenol epigallocatechin-3-gallate on cardiac involvement in patients with AL amyloidosis. *Clin. Res. Cardiol.* **99,** 483–490
36. Solomon, A., and McLaughlin, C. L. (1969) Bence-Jones proteins and light chains of immunoglobulins. I. Formation and characterization of amino-terminal (variant) and carboxyl-terminal (constant) halves. *J. Biol. Chem.* **244,** 3393–3404
37. Liao, R., Jain, M., Teller, P., Connors, L. H., Ngoy, S., Skinner, M., Falk, R. H., and Apstein, C. S. (2001) Infusion of light chains from patients with cardiac amyloidosis causes diastolic dysfunction in isolated mouse hearts. *Circulation* **104,** 1594–1597
38. Shinagawa, A., Kojima, H., Kobayashi, T., Kawada, K., and Nagasawa, T. (2001) Lupus anticoagulant-like activity observed in a dimeric λ protein produced by myeloma cells. *Int. J. Hematol.* **73,** 526–531
39. Schiffer, M., Chang, C. H., and Stevens, F. J. (1985) Formation of an infinite β-sheet arrangement dominates the crystallization behavior of lambda-type antibody light chains. *J. Mol. Biol.* **186,** 475–478
40. Kratzin, H. D., Palm, W., Stangel, M., Schmidt, W. E., Friedrich, J., and Hilschmann, N. (1989) [The primary structure of crystallizable monoclonal immunoglobulin IgG1 Kol. II. Amino acid sequence of the L-chain, γ-type, subgroup I]. *Biol. Chem. Hoppe Seyler* **370,** 263–272

41. Lefranc, M.-P., and Lefranc, G. (2001) *The Immunoglobulin FactsBook*, pp. 17–28, Academic Press, San Diego, CA
42. Cohn, J. R., and Emmett, E. A. (1978) The excretion of trace metals in human sweat. *Ann. Clin. Lab. Sci.* **8,** 270–275
43. Goto, Y., and Hamaguchi, K. (1979) The role of the intrachain disulfide bond in the conformation and stability of the constant fragment of the immunoglobulin light chain. *J. Biochem.* **86,** 1433–1441
44. Blancas-Mejía, L. M., Tischer, A., Thompson, J. R., Tai, J., Wang, L., Auton, M., and Ramirez-Alvarado, M. (2014) Kinetic control in protein folding for light chain amyloidosis and the differential effects of somatic mutations. *J. Mol. Biol.* **426,** 347–361
45. Lefranc, M. P. (2003) IMGT databases, web resources and tools for immunoglobulin and T cell receptor sequence analysis. *Leukemia* **17,** 260–266
46. Klausner, R. D., Kempf, C., Weinstein, J. N., Blumenthal, R., and Van Renswoude, J. (1983) The folding of ovalbumin: renaturation *in vitro versus* biosynthesis *in vitro*. *Biochem. J.* **212,** 801–810
47. Mantulin, W. W., Rohde, M. F., Gotto, A. M., Jr, and Pownall, H. J. (1980) The conformational properties of human plasma apolipoprotein C-II: a spectroscopic study. *J. Biol. Chem.* **255,** 8185–8191
48. Hopkins, T. R., and Spikes, J. D. (1967) Denaturation of proteins in 8 M urea as monitored by tryptophan fluorescence: chymotrypsin, chymotrypsinogen and some derivatives. *Biochem. Biophys. Res. Commun.* **28,** 480–484
49. Bergen, H. R., 3rd, Dasari, S., Dispenzieri, A., Mills, J. R., Ramirez-Alvarado, M., Tschumper, R. C., Jelinek, D. F., Barnidge, D. R., and Murray, D. L. (2016) Clonotypic light chain peptides identified for monitoring minimal residual disease in multiple myeloma without bone marrow aspiration. *Clin. Chem.* **62,** 243–251
50. Maurer-Stroh, S., Debulpaep, M., Kuemmerer, N., Lopez de la Paz, M., Martins, I. C., Reumers, J., Morris, K. L., Copland, A., Serpell, L., Serrano, L., Schymkowitz, J. W., and Rousseau, F. (2010) Exploring the sequence determinants of amyloid structure using position-specific scoring matrices. *Nat. Methods* **7,** 237–242
51. Cohen, S. I., Linse, S., Luheshi, L. M., Hellstrand, E., White, D. A., Rajah, L., Otzen, D. E., Vendruscolo, M., Dobson, C. M., and Knowles, T. P. (2013) Proliferation of amyloid-β42 aggregates occurs through a secondary nucleation mechanism. *Proc. Natl. Acad. Sci. U.S.A.* **110,** 9758–9763
52. Hurshman, A. R., White, J. T., Powers, E. T., and Kelly, J. W. (2004) Transthyretin aggregation under partially denaturing conditions is a downhill polymerization. *Biochemistry* **43,** 7365–7381
53. Chandrashekaran, I. R., Adda, C. G., MacRaild, C. A., Anders, R. F., and Norton, R. S. (2010) Inhibition by flavonoids of amyloid-like fibril formation by *Plasmodium falciparum* merozoite surface protein 2. *Biochemistry* **49,** 5899–5908
54. Chandrashekaran, I. R., Adda, C. G., Macraild, C. A., Anders, R. F., and Norton, R. S. (2011) EGCG disaggregates amyloid-like fibrils formed by *Plasmodium falciparum* merozoite surface protein 2. *Arch. Biochem. Biophys.* **513,** 153–157
55. Grelle, G., Otto, A., Lorenz, M., Frank, R. F., Wanker, E. E., and Bieschke, J. (2011) Black tea theaflavins inhibit formation of toxic amyloid-beta and α-synuclein fibrils. *Biochemistry* **50,** 10624–10636
56. Palhano, F. L., Lee, J., Grimster, N. P., and Kelly, J. W. (2013) Toward the molecular mechanism(s) by which EGCG treatment remodels mature amyloid fibrils. *J. Am. Chem. Soc.* **135,** 7503–7510
57. Andrich, K., and Bieschke, J. (2015) The effect of (−)-epigallo-catechin-(3)-gallate on amyloidogenic proteins suggests a common mechanism. *Adv. Exp. Med. Biol.* **863,** 139–161
58. Mereles, D., Wanker, E. E., and Katus, H. A. (2008) Therapy effects of green tea in a patient with systemic light-chain amyloidosis. *Clin. Res. Cardiol.* **97,** 341–344
59. Blancas-Mejia, L. M., Tellez, L. A., del Pozo-Yauner, L., Becerril, B., Sanchez-Ruiz, J. M., and Fernandez-Velasco, D. A. (2009) Thermodynamic and kinetic characterization of a germ line human λ6 light-chain protein: the relation between unfolding and fibrillogenesis. *J. Mol. Biol.* **386,** 1153–1166
60. Baden, E. M., Randles, E. G., Aboagye, A. K., Thompson, J. R., and Ramirez-Alvarado, M. (2008) Structural insights into the role of mutations in amyloidogenesis. *J. Biol. Chem.* **283,** 30950–30956
61. Baden, E. M., Owen, B. A., Peterson, F. C., Volkman, B. F., Ramirez-Alvarado, M., and Thompson, J. R. (2008) Altered dimer interface decreases stability in an amyloidogenic protein. *J. Biol. Chem.* **283,** 15853–15860
62. Marin-Argany, M., Güell-Bosch, J., Blancas-Mejía, L. M., Villegas, S., and Ramirez-Alvarado, M. (2015) Mutations can cause light chains to be too stable or too unstable to form amyloid fibrils. *Protein Sci.* **24,** 1829–1840
63. Chung, C. M., Chiu, J. D., Connors, L. H., Gursky, O., Lim, A., Dykstra, A. B., Liepnieks, J., Benson, M. D., Costello, C. E., Skinner, M., and Walsh, M. T. (2005) Thermodynamic stability of a κI immunoglobulin light chain: relevance to multiple myeloma. *Biophys. J.* **88,** 4232–4242
64. Arosio, P., Owczarz, M., Müller-Späth, T., Rognoni, P., Beeg, M., Wu, H., Salmona, M., and Morbidelli, M. (2012) *In vitro* aggregation behavior of a non-amyloidogenic λ light chain dimer deriving from U266 multiple myeloma cells. *PLoS One* **7,** e33372
65. Blancas-Mejía, L. M., and Ramirez-Alvarado, M. (2016) Recruitment of light chains by homologous and heterologous fibrils shows distinctive kinetic and conformational specificity. *Biochemistry* **55,** 2967–2978
66. Brumshtein, B., Esswein, S. R., Salwinski, L., Phillips, M. L., Ly, A. T., Cascio, D., Sawaya, M. R., and Eisenberg, D. S. (2015) Inhibition by small-molecule ligands of formation of amyloid fibrils of an immunoglobulin light chain variable domain. *eLife* **4,** e10935
67. Bergen, H. R., 3rd, Abraham, R. S., Johnson, K. L., Bradwell, A. R., and Naylor, S. (2004) Characterization of amyloidogenic immunoglobulin light chains directly from serum by on-line immunoaffinity isolation. *Biomed. Chromatogr.* **18,** 191–201
68. Feige, M. J., Hagn, F., Esser, J., Kessler, H., and Buchner, J. (2007) Influence of the internal disulfide bridge on the folding pathway of the CL antibody domain. *J. Mol. Biol.* **365,** 1232–1244
69. Tsunenaga, M., Goto, Y., Kawata, Y., and Hamaguchi, K. (1987) Unfolding and refolding of a type κ immunoglobulin light chain and its variable and constant fragments. *Biochemistry* **26,** 6044–6051
70. Glenner, G. G., Ein, D., Eanes, E. D., Bladen, H. A., Terry, W., and Page, D. L. (1971) Creation of "amyloid" fibrils from Bence Jones proteins *in vitro*. *Science* **174,** 712–714
71. Garai, K., and Frieden, C. (2013) Quantitative analysis of the time course of Aβ oligomerization and subsequent growth steps using tetramethylrhodamine-labeled Aβ. *Proc. Natl. Acad. Sci. U.S.A.* **110,** 3321–3326
72. Lee, J., Culyba, E. K., Powers, E. T., and Kelly, J. W. (2011) Amyloid-β forms fibrils by nucleated conformational conversion of oligomers. *Nat. Chem. Biol.* **7,** 602–609
73. Gupta, P., and Deep, S. (2015) Salt mediated unusual switching in the aggregation kinetic profile of human carbonic anhydrase. *RSC Adv.* **5,** 95717–95726
74. Balch, W. E., Morimoto, R. I., Dillin, A., and Kelly, J. W. (2008) Adapting proteostasis for disease intervention. *Science* **319,** 916–919
75. Baumstark, J. S. (1983) Guidelines for the preparative fractionation of human serum proteins on gradient-eluted columns of concanavalin A-Sepharose: elution positions of fourteen well-characterized proteins and evidence for concanavalin A-reactive albumin-IgA and -IgG complexes. *Prep. Biochem.* **13,** 315–345
76. Sengupta, S., Chen, H., Togawa, T., DiBello, P. M., Majors, A. K., Büdy, B., Ketterer, M. E., and Jacobsen, D. W. (2001) Albumin thiolate anion is an intermediate in the formation of albumin-S-S-homocysteine. *J. Biol. Chem.* **276,** 30111–30117
77. Caruana, M., Högen, T., Levin, J., Hillmer, A., Giese, A., and Vassallo, N. (2011) Inhibition and disaggregation of α-synuclein oligomers by natural polyphenolic compounds. *FEBS Lett.* **585,** 1113–1120
78. Sinha, S., Du, Z., Maiti, P., Klärner, F. G., Schrader, T., Wang, C., and Bitan, G. (2012) Comparison of three amyloid assembly inhibitors: the sugar scyllo-inositol, the polyphenol epigallocatechin gallate, and the molecular tweezer CLR01. *ACS Chem. Neurosci.* **3,** 451–458
79. Gauci, A. J., Caruana, M., Giese, A., Scerri, C., and Vassallo, N. (2011) Identification of polyphenolic compounds and black tea extract as potent inhibitors of lipid membrane destabilization by Aβ(4)(2) aggregates. *J. Alzheimers Dis.* **27,** 767–779
80. Pelaez-Aguilar, A. E., Rivillas-Acevedo, L., French-Pacheco, L., Valdes-Garcia, G., Maya-Martinez, R., Pastor, N., and Amero, C. (2015) Inhibition

of light chain 6aJL2-R24G amyloid fiber formation associated with light chain amyloidosis. *Biochemistry* **54,** 4978–4986
81. Wobst, H. J., Sharma, A., Diamond, M. I., Wanker, E. E., and Bieschke, J. (2015) The green tea polyphenol (−)-epigallocatechin gallate prevents the aggregation of tau protein into toxic oligomers at substoichiometric ratios. *FEBS Lett.* **589,** 77–83
82. Lopez del Amo, J. M., Fink, U., Dasari, M., Grelle, G., Wanker, E. E., Bieschke, J., and Reif, B. (2012) Structural properties of EGCG-induced, nontoxic Alzheimer's disease Aβ oligomers. *J. Mol. Biol.* **421,** 517–524
83. Lee, Y. K., Yuk, D. Y., Lee, J. W., Lee, S. Y., Ha, T. Y., Oh, K. W., Yun, Y. P., and Hong, J. T. (2009) (−)-Epigallocatechin-3-gallate prevents lipopolysaccharide-induced elevation of β-amyloid generation and memory deficiency. *Brain Res.* **1250,** 164–174
84. Wang, S. H., Dong, X. Y., and Sun, Y. (2012) Thermodynamic analysis of the molecular interactions between amyloid β-protein fragments and (−)-epigallocatechin-3-gallate. *J. Phys. Chem. B* **116,** 5803–5809
85. Wang, S. H., Liu, F. F., Dong, X. Y., and Sun, Y. (2010) Thermodynamic analysis of the molecular interactions between amyloid β-peptide 42 and (−)-epigallocatechin-3-gallate. *J. Phys. Chem. B* **114,** 11576–11583
86. Bieschke, J., Herbst, M., Wiglenda, T., Friedrich, R. P., Boeddrich, A., Schiele, F., Kleckers, D., Lopez del Amo, J. M., Grüning, B. A., Wang, Q., Schmidt, M. R., Lurz, R., Anwyl, R., Schnoegl, S., Fändrich, M., *et al.* (2012) Small-molecule conversion of toxic oligomers to nontoxic β-sheet-rich amyloid fibrils. *Nat. Chem. Biol.* **8,** 93–101
87. Sun, T., Lien, Y. Y., and Degnan, T. (1979) Study of gammopathies with immunofixation electrophoresis. *Am. J. Clin. Pathol.* **72,** 5–11
88. Ehrenmann, F., Kaas, Q., and Lefranc, M. P. (2010) IMGT/3Dstructure-DB and IMGT/DomainGapAlign: a database and a tool for immunoglobulins or antibodies, T cell receptors, MHC, IgSF and MhcSF. *Nucleic Acids Res.* **38,** D301–D307
89. Ruiz, M., and Lefranc, M. P. (2002) IMGT gene identification and Colliers de Perles of human immunoglobulins with known 3D structures. *Immunogenetics* **53,** 857–883
90. Kaas, Q., Ehrenmann, F., and Lefranc, M. P. (2007) IG, TR and IgSF, MHC and MhcSF: what do we learn from the IMGT Colliers de Perles? *Brief Funct. Genomic Proteomic* **6,** 253–264
91. Greene, R. F., Jr., and Pace, C. N. (1974) Urea and guanidine hydrochloride denaturation of ribonuclease, lysozyme, α-chymotrypsin, and β-lactoglobulin. *J. Biol. Chem.* **249,** 5388–5393

Aggregation of Full-length Immunoglobulin Light Chains from Systemic Light Chain Amyloidosis (AL) Patients Is Remodeled by Epigallocatechin-3-gallate

Kathrin Andrich, Ute Hegenbart, Christoph Kimmich, Niraja Kedia, H. Robert Bergen, 3rd, Stefan Schönland, Erich Wanker and Jan Bieschke

J. Biol. Chem. 2017, 292:2328-2344.
doi: 10.1074/jbc.M116.750323 originally published online December 28, 2016

Aggregation of full length immunoglobulin light chains from AL Amyloidosis patients is remodeled by Epigallocatechin-3-gallate

Kathrin Andrich[1,2], Ute Hegenbart[3], Christoph Kimmich[3], Niraja Kedia[1], H. Robert Bergen 3rd [4], Stefan Schönland[3], Erich Wanker[2] and Jan Bieschke[1*]

1) Department of Biomedical Engineering, Washington University in St. Louis, St. Louis, Missouri 63130-4899, USA, 2) Max-Delbrück Center for Molecular Medicine in the Helmholtz Association, 13125 Berlin, Germany, 3) University Hospital Heidelberg, Department of Internal Medicine V (Hematology / Amyloidosis Center) Heidelberg, 69120, Germany

Running title: *LC aggregation and EGCG*

*To whom correspondence should be addressed: bieschke@wustl.edu

Keywords: AL Amyloidosis, Multiple Myeloma, monoclonal gammopathy, proteinuria, immunoglobulin light chain, protein aggregation, amyloid, circular dichroism, tryptophan fluorescence, gel electrophoresis

---

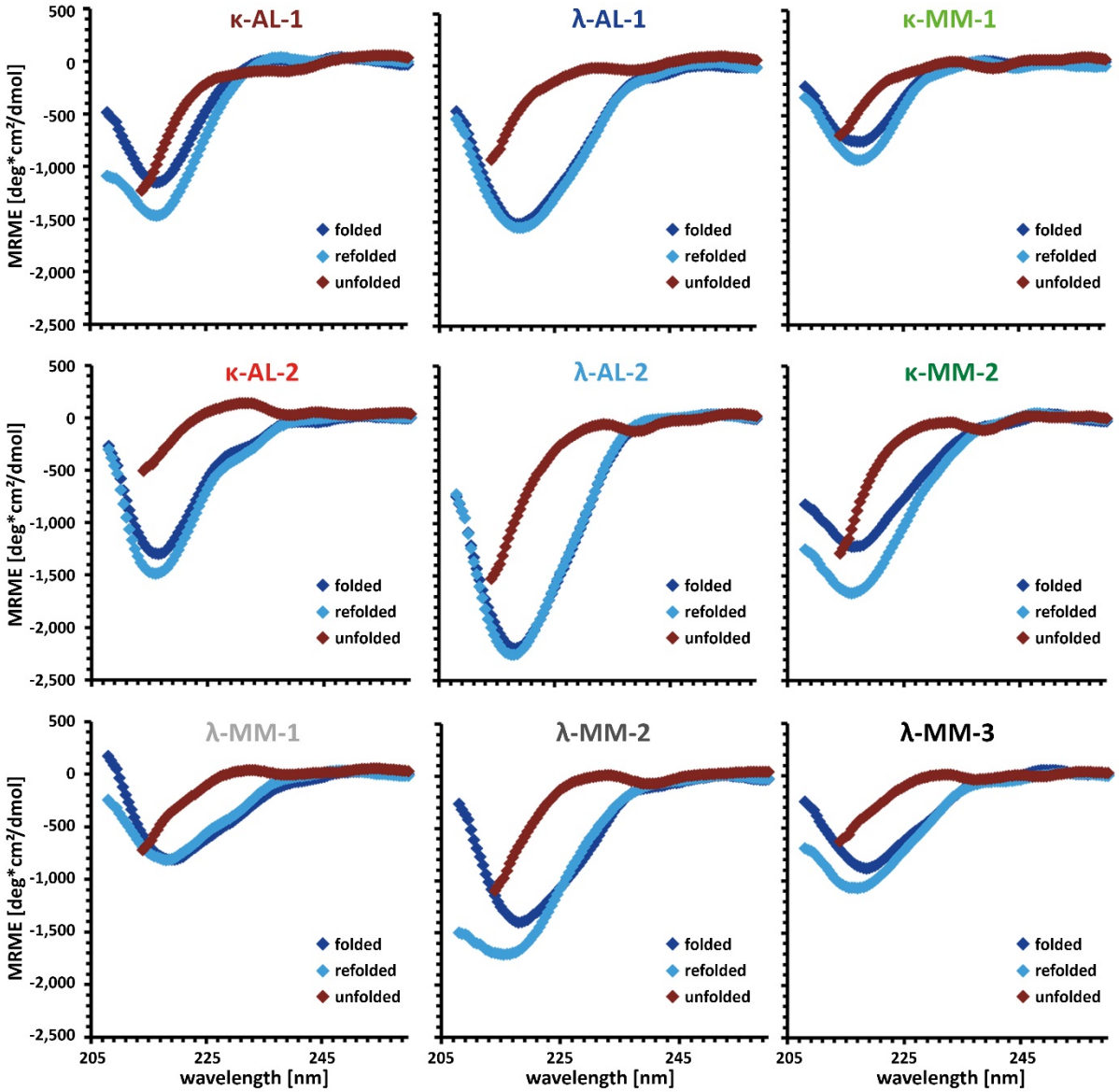

Supplementary Figure 1
Reversibility of GdnHCl denaturation. CD spectra of LC samples under native conditions (folded), in 6M GdnHCl (unfolded) and LC diluted from 6M GdnHCl to 60 mM GdnHCl (refolded).

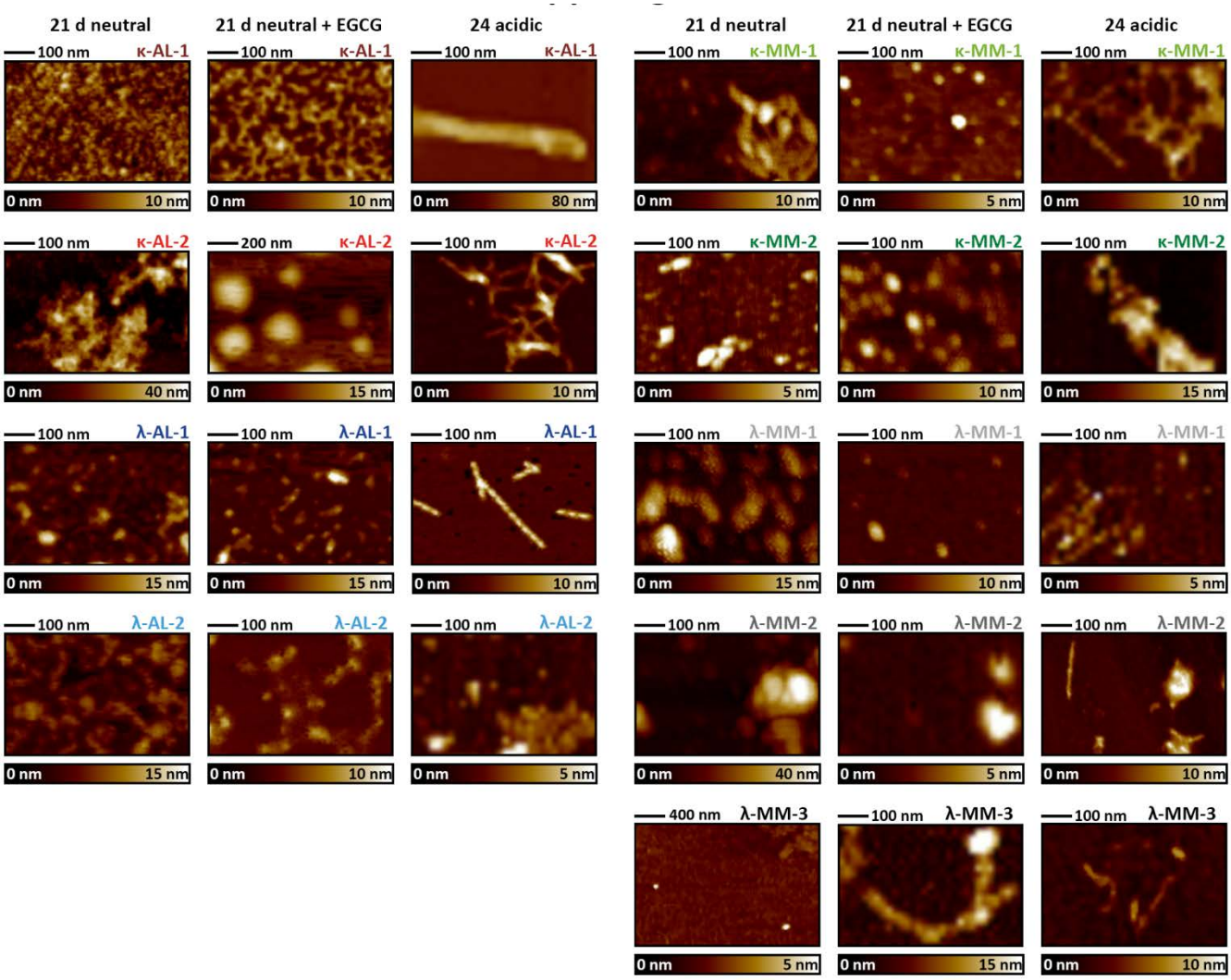

Supplementary Figure 2
AFM imaging of long-term aggregation assay with permanent shaking for 21 days under neutral conditions in absence or presence of equimolar EGCG (Compare to Fig. 4, 5, 8, and 9) or for 24 days under acidic conditions (25 µM LC, 50 mM Glycine / HCl pH 2.8, 150 mM NaCl, 0.05% NaN_3, 100 mM DTT, 20 µM ThT).

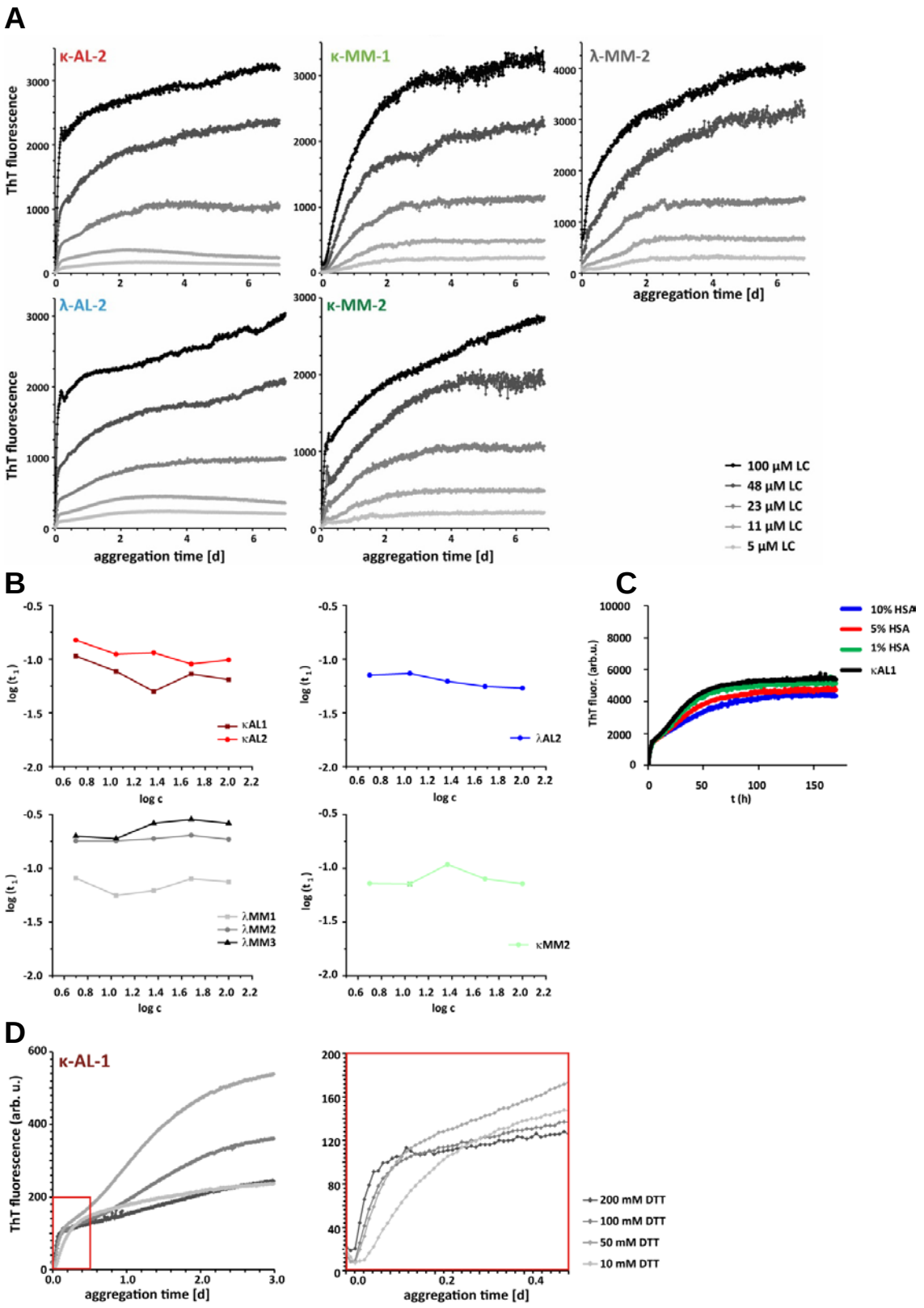

Supplementary Figure 3

A) Supplementary kinetics for Fig. 6*B* - ThT aggregation kinetics at different LC protein concentrations. Samples show biphasic aggregation kinetics. B) First phase time constants for biphasic aggregation fits. Concentrations 11 µM and 5µM of λ-AL-1LC were fitted without a first aggregation phase. C) κ-AL-1 LC aggregation kinetics in presence of 0.2, 1, and 2 µM HSA. ThT fluorescence from HSA samples without LC was subtracted to generate LC ThT fluorescence kinetics. The presence of HSA slightly delayed the second aggregation phase of LC kinetics, but had no effect on the first phase. All plots represent averages of triplicate

samples. D) DTT-dependent aggregation kinetics – Aggregation kinetics performed under standard conditions, at DTT concentrations of 10, 50, 100, and 200 mM. The first aggregation phase is accelerated by increasing DTT concentrations. All plots represent averages of triplicate samples.

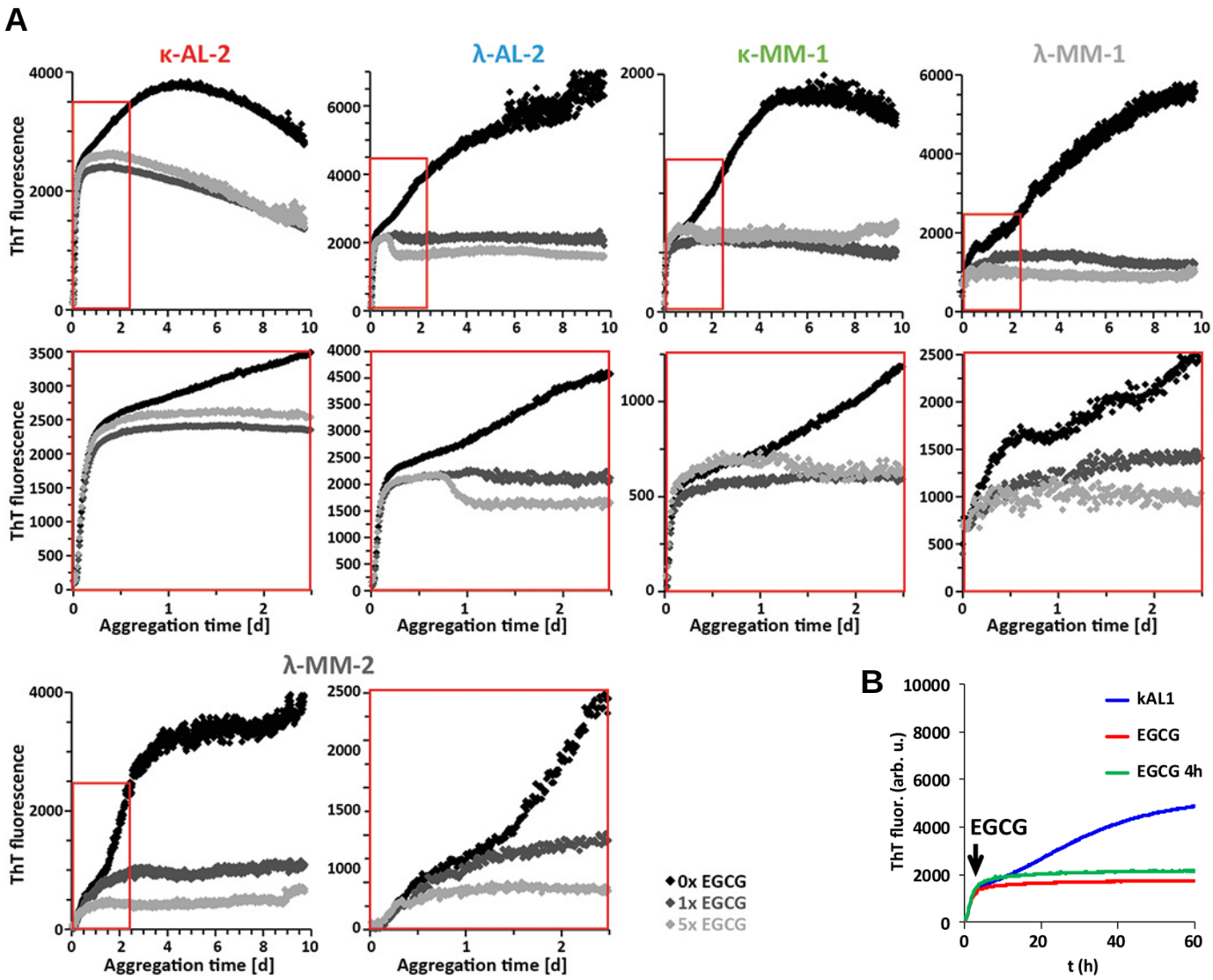

Supplementary Figure 4
Supplementary kinetics for Fig. 7 – A) ThT kinetics in absence (0x) of EGCG, with equimolar EGCG (1x) and five-fold excess EGCG (5x) in relation to the LC concentration. EGCG prevented formation of ThT positive species in the second aggregation phase; full kinetics & zoom of the first 2.5 days of aggregation. All plots represent averages of triplicate samples. B) κ-AL-1 LC (25 μM, NaP buffer pH 7.4) aggregation kinetics in absence (0x) of EGCG, with equimolar EGCG (1x) added at the beginning of the assay or after 4 h incubation. EGCG prevented formation of ThT positive species in the second aggregation phase.